Title

Chloroplast Chaperonin-Mediated Targeting of a Thylakoid Membrane Protein

Journal

The Plant Cell, 32(12)

ISSN

1040-4651

Authors

Klasek, Laura

Inoue, Kentaro

Theg, Steven M

Publication Date

2020-12-01

DOI

10.1105/tpc.20.00309

Peer reviewed

The Plant Cell, Vol. 32: 3884–3901, December 2020, www.plantcell.org © 2020 ASPB.

Chloroplast Chaperonin-Mediated Targeting of a Thylakoid Membrane Protein

Laura Klasek,[a] Kentaro Inoue,[b] and Steven M. Theg[a,1]

[a] Department of Plant Biology, University of California Davis, Davis, California 95616
[b] Department of Plant Sciences, University of California Davis, Davis, California 95616

ORCID IDs: 0000-0002-5432-1809 (L.K.); 0000-0001-5604-2486 (K.I.); 0000-0002-6397-0413 (S.M.T.)

Posttranslational protein targeting requires chaperone assistance to direct insertion-competent proteins to integration pathways. Chloroplasts integrate nearly all thylakoid transmembrane proteins posttranslationally, but mechanisms in the stroma that assist their insertion remain largely undefined. Here, we investigated how the chloroplast chaperonin (Cpn60) facilitated the thylakoid integration of Plastidic type I signal peptidase 1 (Plsp1) using in vitro targeting assays. Cpn60 bound Plsp1 in the stroma. In isolated chloroplasts, the membrane integration of imported Plsp1 correlated with its dissociation from Cpn60. When the Plsp1 residues that interacted with Cpn60 were removed, Plsp1 did not integrate into the membrane. These results suggested Cpn60 was an intermediate in thylakoid targeting of Plsp1. In isolated thylakoids, the integration of Plsp1 decreased when Cpn60 was present in excess of cpSecA1, the stromal motor of the cpSec1 translocon that inserts unfolded Plsp1 into the thylakoid. An excess of cpSecA1 favored integration. Introducing Cpn60's obligate substrate RbcL displaced Cpn60-bound Plsp1; then, the released Plsp1 exhibited increased accessibility to cpSec1. These in vitro targeting experiments support a model in which Cpn60 captures and then releases insertion-competent Plsp1, whereas cpSecA1 recognizes free Plsp1 for integration. Thylakoid transmembrane proteins in the stroma can interact with Cpn60 to shield themselves from the aqueous environment.

INTRODUCTION

In oxygenic photosynthesis, the light-harvesting reactions and ATP synthesis occur at the thylakoid, the internal membrane of chloroplasts and cyanobacteria. Thylakoid development requires coordinated synthesis, delivery, and assembly of its proteins, pigments, and lipids (Rast et al., 2015). Cotranslational integration is the predominant mechanism for inserting membrane proteins into a lipid bilayer when translation and integration are spatially coupled. This cotranslational integration process targets an estimated 86% and 75% of membrane proteins to the *Escherichia coli* plasma membrane and yeast (*Saccharomyces cerevisiae*) endoplasmic reticulum, respectively (del Alamo et al., 2011; Schibich et al., 2016). Ribosomes decorate thylakoids in cyanobacteria (Rast et al., 2019), suggesting cotranslational integration of cyanobacterial thylakoid proteins as well. However, in plants, the nuclear genome encodes the majority of integral thylakoid transmembrane (TM) proteins, and the plastid genome encodes about 40 TM proteins. Of ~170 thylakoid proteins with at least one predicted TM domain (TMD), only 10% integrate cotranslationally (Sun et al., 2009; Zoschke and Barkan, 2015). Thus, chloroplasts depend upon posttranslational mechanisms to deliver thylakoid TM proteins.

To facilitate its posttranslational targeting, a thylakoid TM protein may need to be folded or kept unfolded in the stroma. The chloroplast secretory (cpSec1) and signal recognition particle (cpSRP) pathways both insert unfolded proteins into the thylakoid (Klasek and Inoue, 2016). During in vitro targeting assays, premature folding of the cpSec1 substrate Plastidic type I signal peptidase 1 (Plsp1; Paetzel, 2014) mistargets Plsp1 to the stromal face of the thylakoid (Endow et al., 2015). The cpSRP substrate light-harvesting complex protein (LHCP) rapidly aggregates (Payan and Cline, 1991; Jaru-Ampornpan et al., 2010). The chloroplast must chaperone unfolded thylakoid TM proteins transiting the stroma.

An unfolded, insertion-competent state can be stabilized by either specific targeting factors or promiscuous chaperones. In *E. coli*, the SecB targeting factor keeps secreted proteins unfolded (Sala et al., 2014). The cytosolic Guided Entry of Tail-anchored proteins (GET) pathway targets tail-anchored proteins to the endoplasmic reticulum via a cascade of chaperones that increase in specificity for insertion-competent tail-anchored substrates (Shan, 2019). In contrast, the mechanisms that stabilize thylakoid proteins in transit are largely unknown beyond two specific examples. First, the plastid-specific cpSRP43 targeting factor assists LHCP in transiting the stroma by preventing and reversing its aggregation (Payan and Cline, 1991; Jaru-Ampornpan et al., 2010). Second, the chloroplast Hsp90 chaperone promotes the thylakoid association of cpSec1-targeted OE33/PsbO (Jiang et al., 2017). In addition, the stromal chaperones Cpn60, ClpC/Hsp93, Hsp70, and Hsp90 all interact with newly imported proteins (Lubben et al., 1989; Madueno et al., 1993; Tsugeki and Nishimura, 1993; Bonk et al., 1997; Shi and Theg, 2010; Su and Li, 2010; Rosano et al., 2011; Inoue et al., 2013; Huang et al., 2016). These chaperones could, in principle, stabilize thylakoid TM proteins in the stroma.

[1] Address correspondence to smtheg@ucdavis.edu.
The author responsible for distribution of materials integral to the findings presented in this article in accordance with the policy described in the Instructions for Authors (www.plantcell.org) is: Steven M. Theg (smtheg@ucdavis.edu).
www.plantcell.org/cgi/doi/10.1105/tpc.20.00309

IN A NUTSHELL

Background: As a plant grows, its chloroplasts construct their internal thylakoid membranes to begin harvesting light for photosynthesis. The thylakoid is protein-rich, and most of its proteins are translated in the cytosol. Once the chloroplast recognizes and takes up these proteins, additional chaperones help them cross the stroma to reach the growing thylakoid. However, which chaperones help what particular thylakoid membrane protein is mostly unknown. Plastidic type I signal peptidase 1 (Plsp1) is a thylakoid membrane protein that must stay unfolded in the stroma until it reaches the thylakoid. We observed Plsp1 in a large stromal protein complex that resembled a chaperone (Cpn60) known for helping proteins fold.

Questions: Does Plsp1 interact directly with Cpn60 and, if so, does Cpn60 help Plsp1 cross the stroma to reach the thylakoid membrane?

Findings: We found that Cpn60 binds and releases Plsp1, which can then be delivered to the thylakoid. When we isolated chloroplasts from pea seedlings and let them take up Arabidopsis Plsp1 containing radioactive amino acids, we saw the radiolabeled signal first in the Cpn60-Plsp1 complex, then later in the thylakoid membrane. Cpn60 interacts with many stromal proteins, including the large subunit of Rubisco (RbcL). When we added RbcL and ATP to Cpn60-Plsp1 complexes, Cpn60 released Plsp1 and bound RbcL. If we added RbcL to Cpn60-Plsp1 complexes in the presence of thylakoids and the machinery which inserts Plsp1, Plsp1 reached the thylakoid successfully.

Next steps: Open questions from our work include determining how important Cpn60 is for enabling Plsp1 to reach the thylakoid and whether Cpn60 assists other thylakoid proteins. Better understanding of Cpn60 and of thylakoid development will enable more nuanced strategies to improve how plants use light.

Of these, the chaperonin (Cpn60) is a seemingly unlikely candidate to assist cpSec1-mediated targeting of unfolded proteins. Chaperonins bind nonnative proteins and ATP within one heptameric ring of a barrel-shaped tetradecameric oligomer (Hayer-Hartl et al., 2016; Zhao and Liu, 2018). Cpn60 is a heterooligomer of distinct α and β 60-kD subunits (Musgrove et al., 1987; Nishio et al., 1999). In angiosperms, Cpn60 α further diversified into α1 and α2 isoforms, whereas Cpn60 β diversified into β1 and β4 isoforms (Zhao and Liu, 2018). Why Cpn60 has so many isoforms remains unclear, but mounting evidence suggests that different isoforms recognize distinct substrates (Peng et al., 2011; Ke et al., 2017; Zhao and Liu, 2018). Chaperonins encapsulate bound proteins within one ring in cooperation with a cochaperonin lid (Hayer-Hartl et al., 2016). ATP hydrolysis within the occupied ring and nonnative protein binding to the opposite ring release the encapsulated protein. A released protein may rebind until it achieves a native conformation (Liu et al., 2010; Gruber and Horovitz, 2016; Hayer-Hartl et al., 2016). Chaperonins fold essential proteins in chloroplasts, mitochondria, and bacteria, as does the related group II chaperonin (CCT/TRiC) found in the eukaryotic cytosol (Kerner et al., 2005; Yam et al., 2008; Zhao and Liu, 2018; Bie et al., 2020). Though some biochemical and genetic evidence suggests *E. coli* GroEL (Castanié-Cornet et al., 2014) and mammalian cytosolic CCT/TRiC (Génier et al., 2016) play a role in targeting, all known functions of Cpn60 involve the folding of stromal proteins.

The nuclear-encoded TM protein Plsp1 localizes to the envelope in meristematic plastids, then increasingly to thylakoids as the chloroplast develops (Shipman and Inoue, 2009). Plsp1 derives from the endosymbiont (Hsu et al., 2011). Plsp1's *E. coli* homolog (de Gier et al., 1996; Valent et al., 1998) and presumably its cyanobacterial progenitor insert cotranslationally, but Plsp1 integrates posttranslationally into the envelope by an unknown mechanism and into the thylakoid via the cpSec1 translocon (Endow et al., 2015). During its targeting, Plsp1 transiently resides in the stroma in a 700-kD complex that is hypothesized to assist its targeting to the thylakoid (Endow et al., 2015). The size and ATP-mediated dissociation of this complex suggested that it represents an interaction between Plsp1 and Cpn60 (Endow et al., 2015). In this work, we demonstrate that Plsp1 interacts with Cpn60 via sequences immediately adjacent to its thylakoid targeting signal and characterize the mechanism by which Cpn60 captures and releases Plsp1 during thylakoid targeting.

RESULTS

Plsp1 Interacts with Cpn60

Cpn60 migrates in an ~700-kD complex that dissociates upon ATP treatment, the same size and behavior observed of Plsp1's stromal complex (Hemmingsen and Ellis, 1986; Endow et al., 2015). To confirm that the comigration of Cpn60 and Plsp1's stromal complex indeed represented direct interaction between Cpn60 and Plsp1, we determined which stromal proteins Plsp1 binds by an in vitro pulldown assay. Two sequential elution steps were tested to determine, first, what was released from binding Plsp1 by ATP treatment, which disrupted the stromal complex containing Plsp1 (Endow et al., 2015), and second, what proteins eluted with Plsp1. The Plsp1 variant (mPlsp1$_{\Delta TMD}$) used as the bait protein lacks its transit peptide and TMD, which were previously shown to be dispensable for formation of the 700-kD complex (Endow et al., 2015). As negative controls, we chose both the model cpSec1 substrate OE33, which does not interact with Cpn60 (Molik et al., 2001), and a mock pulldown lacking a bait protein. When incubated with freshly prepared SE, Plsp1 pulled down Cpn60. This Cpn60 was partially released by ATP treatment when Plsp1, but not OE33, was the pulldown bait (Figure 1A, lane 6). More Cpn60 eluted with Plsp1 (Figure 1A, lane 8). In contrast, OE33 eluted with considerably less than 1% of input Cpn60

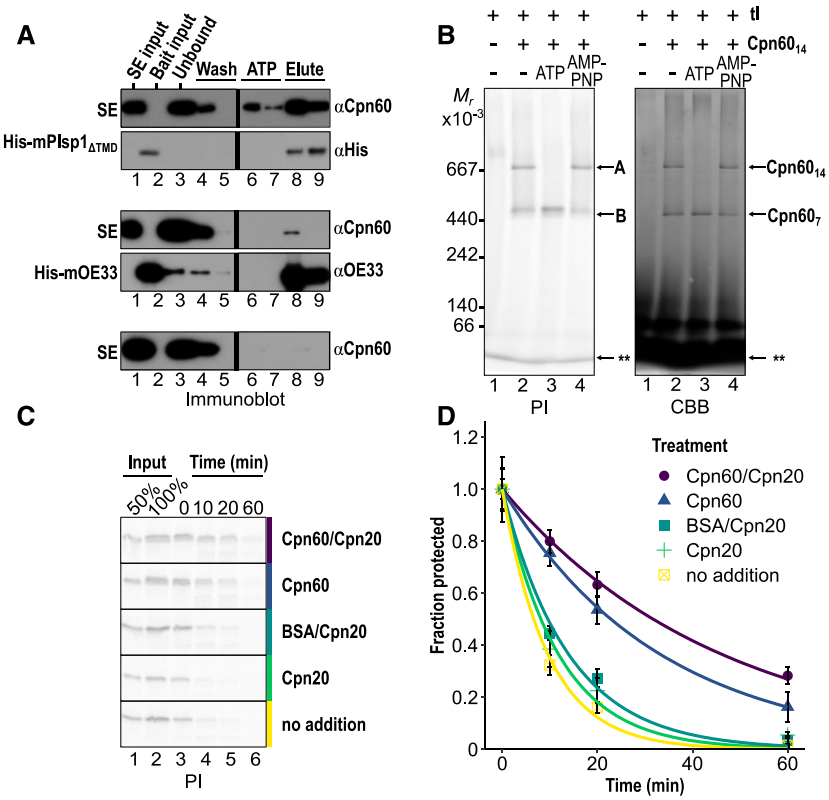

Figure 1. Plsp1 Directly Interacts with Cpn60 α1 and β1.

(A) In vitro pulldown of Cpn60 from SE with His-tagged bait. The three pairs of blots represent assays with mPlsp1$_{\Delta TMD}$ and SE (top pair), mOE33 and SE (middle pair), and SE alone without bait protein (bottom pair). Twenty micrograms bait proteins were incubated with SE equivalent to 250 μg chlorophyll (Chl), then bound to affinity resin, washed, and sequentially treated with 10 mM ATP and 300 mM imidazole. Representative immunoblots of three independent experiments show (in lanes 1 to 9): 1% of SE input, 2.5% of bait input, 1% of unbound, and 25% of two washes, ATP treatment (ATP), and imidazole elution (elute). Black lines mark lanes removed (three additional washes). Cpn60 was detected with anti-(α)Hsp60, His-mPlsp1$_{\Delta TMD}$ with anti-His, and His-mOE33 with anti-OE33 antibodies. Bait proteins were not detected for the SE control.

(B) Cpn60 tetradecamer binding assay. In vitro-translated, radiolabeled mPlsp1 (tl) was incubated with 250 nM Cpn60 tetradecamer (Cpn60$_{14}$) for 30 min at room temperature. Ten millimolar ATP or AMP-PNP were added (where indicated by + or −) for an additional 10 min incubation. The binding assay was separated via 4 to 14% BN-PAGE. Radiolabeled proteins were visualized by autoradiography and phosphorimaging (left, PI), and Cpn60 oligomers were visualized by Coomassie staining (right, CBB). The observed radiolabeled bands detected by autoradiography at 700 kD and just above 440 kD are labeled A and B, respectively. Cpn60$_{14}$ and Cpn60$_7$ indicate the sizes of tetradecameric and heptameric Cpn60 oligomers, respectively. Asterisks (**) indicate monomeric mPlsp1, which migrates with the dye front. A representative gel from three independent experiments with similar results is shown.

(C) Proteinase K protection assay of Cpn60-mediated substrate encapsulation. In vitro-translated, radiolabeled Plsp1 was incubated with Cpn60$_{14}$ (0.8 μM oligomer, 11.2 μM monomer), BSA (11.2 μM, equivalent to Cpn60 monomer concentration), or buffer for 30 min at room temperature to allow Plsp1 to bind. ADP and, where indicated, Cpn20$_4$ (2 μM), were added, followed by 10 min of further incubation. The assay was initiated with the addition of 1.2 μg/mL proteinase K, and aliquots were removed at 0, 10, 20, and 60 min and quenched with PMSF. After separation on SDS-PAGE, radiolabeled Plsp1 was visualized by autoradiography. Gel phosphorimages (PI) shown are representative of $n = 6$ (no addition) or $n = 7$ (all other treatments) independent digestions.

(D) Quantification of **(C)**. Protection at each time point for each treatment was quantified relative to the zero-minute time point. Points represent means; error bars represent ± 1 SD. Lines represent single-exponential curves ($y = e^{-kt}$) fit to data by least-squares regression.

(Figure 1A, compare lanes 1 and 8). These results indicate that Cpn60 interacted directly and specifically with Plsp1.

The specific Cpn60 isoforms and other stromal proteins pulled down by Plsp1 were identified by liquid chromatography-mass spectrometry (LC-MS)/MS. Proteomic analysis demonstrated that the proteins eluted with Plsp1 (Figure 1A, lane 8) included Cpn60α1 and three β1 isoforms of Cpn60 (Table 1). The minor Cpn60α2 and β4 isoforms and the cochaperonins Cpn20 and Cpn10 were not pulled down to an appreciable degree (Table 1). An additional stromal chaperone, Hsp70, was also pulled down by Plsp1. The Hsp70 $\log_2$ fold change of 4.7 represented a statistically significant 25-fold enrichment in the pulled-down material compared to the control (Table 1). However, Cpn60 was pulled down in near stoichiometric amounts, but Hsp70 was only 1.6% of the Cpn60 pulled down (Table 1; Supplemental Data Set 1). The bulk of stromal Hsp70 did not comigrate with the Plsp1 700-kD

Table 1. Stromal Chaperones Pulled Down by Plsp1

Name	*Pisum sativum* Gene ID	Fold Change	Enriched	% Relative to Total Cpn60	Coverage (%)
Chaperonins and Cochaperonins					
Cpn60 α1	Psat7g144320	8.2	+	48.9	65.9
Cpn60 α2	Psat7g128880	Not identified in LC-MS/MS data			
Cpn60 β1	Psat1g001680	8.3	+	50.9	68.1
Cpn60 β1	Psat0s764g0040	5.2	+		63.2
Cpn60 β1	Psat6g016920	‡	+		70.4
Cpn60 β4	Psat2g080360	‡	—	0.2	15.9
Cpn20	Psat4g019040	3.0	—	0.2	27.7
Cpn10		Not identified in LC-MS/MS data			
Chaperones and Targeting					
Hsp70	Psat1g222760	4.7	+	1.6	40.6
Hsp90	Psat2g102720	1.1	—	0.1	12.3
ClpC	Psat7g039080	0.3	—	0.5	26.2

LC-MS/MS analysis of proteins pulled down by Plsp1 (Figure 1A, lane 8). The average fold change between pulldown (mPlsp1$_{\Delta TMD}$ bait) and control (SE-only mock) was calculated from the $\log_2$ transformed ratio of intensity-based absolute quantification (iBAQ) values for each protein. The ‡ sign indicates detection solely in the pulldown. Enriched (+) indicates proteins that were significantly more abundant in the pulldown than the control; enrichment was determined by Student's *t* test ($p < 0.05$) with correction for multiple comparisons. The % relative to total Cpn60 was calculated using the total iBAQ value for all detected Cpn60 isoforms. The three highly similar Cpn60 β1 isoforms were combined for the % relative to total Cpn60 calculation due to difficulty distinguishing isoforms. Nine additional enriched proteins, none of which amounted to greater than 0.5% of the total Cpn60, were excluded from this table due to their low abundance. Detailed data for all detected proteins are in Supplemental Data Set 1. Data are from $n = 2$ independent experiments.

complex (Endow et al., 2015). These data suggest that although Hsp70 can interact with Plsp1, Hsp70 is unlikely to be responsible for the observed stromal complex. Nine additional proteins were pulled down by Plsp1; however, these proteins were minimally abundant as compared to Cpn60 (Supplemental Data Set 1). We cannot exclude the possibility that further stromal proteins interact with Plsp1's TMD. From this in vitro pulldown, we conclude that Plsp1 directly interacts with Cpn60α1 and β1.

We tested if isolated Cpn60 tetradecamers (Cpn60$_{14}$) and in vitro translated, radiolabeled Plsp1 were sufficient to reconstitute the 700-kD complex. Cpn60$_{14}$, prepared from pea (*Pisum sativum*) and Cpn60α1 and β1 prepared by established procedures (Dickson et al., 2000) was incubated with radiolabeled Plsp1 and examined by blue native-PAGE (BN-PAGE). Two prominent bands of radiolabeled Plsp1 were detected, migrating just above the 669- and 440-kD markers (Figure 1B, labeled A and B). Band A is the same size as the Plsp1 700-kD stromal complex and comigrates with the Cpn60$_{14}$ band detected by Coomassie staining. Band B corresponds approximately in size to a single-ring Cpn60 oligomer (Cpn60$_7$) and comigrates with a fainter Coomassie-staining band. Mitochondrial Hsp60 has active single- and double-ring forms (Weiss et al., 2016), but an active Cpn60$_7$ has not been previously described. Band A disappeared in the presence of hydrolysable ATP, consistent with the observed behavior of the stromal 700-kD complex (Endow et al., 2015). Ten millimolar ATP disrupted formation of band A (Figure 1B, lane 3), while 10 mM AMP-PNP had no effect (lane 4). Band B increased in intensity upon 10 mM ATP treatment, as did its comigrating Cpn60$_7$ band. We conclude that Cpn60α1, Cpn60β1, and Plsp1 interact to form a complex equal in size and similar in behavior to that observed on import into chloroplasts.

Chaperonin interaction conveys protection of its substrates from proteinase K digestion, especially in the presence of a cochaperonin, because the substrate is encapsulated within the chaperonin's cavity beneath the cochaperonin lid (Weissman et al., 1995; Mao et al., 2015). We used this property to further validate that Plsp1 interacts with Cpn60. Radiolabeled Plsp1 was incubated with Cpn60$_{14}$, BSA, or buffer to allow Plsp1 to bind, and then supplemented with Cpn20 (where indicated). BSA incubation served as a control for slow degradation under a high protein load. After the addition of proteinase K, samples were removed at 0, 10, 20, and 60 min, and the fraction of remaining Plsp1 assessed (Figures 1C and 1D). At all time points, Plsp1 exhibited partial resistance to degradation in the presence of Cpn60 as compared to all controls (Figure 1C). Cpn20 alone did not protect Plsp1 but had a small additive effect on the protection due to Cpn60 under these conditions (Figure 1D). The higher level of protection of Plsp1 in the presence of Cpn60$_{14}$ than in the presence of equimolar BSA demonstrated that the protection of Plsp1 was due to Cpn60 interaction specifically, not the protein concentration of the reaction (Figures 1C and 1D). The presence or absence of the Plsp1 transit peptide did not alter its protection by Cpn60 (Supplemental Figure 1). Collectively, these data support the conclusion that Cpn60 encapsulates Plsp1.

The Dissociation of the 700-kD Complex Correlates with Increased Membrane Integration

Plsp1 transiently resides in the stroma prior to its integration into thylakoids by cpSec1, and interaction with Cpn60 may be an intermediate step in targeting of Plsp1 (Endow et al., 2015). We expanded the import-chase assay from our previous study to

examine how the interaction of Plsp1 with Cpn60 correlates with its membrane integration. To generate a pulse of Plsp1, Plsp1 was imported for 10 min, then unincorporated Plsp1 was degraded with membrane-impermeable thermolysin. Chloroplasts were returned to import conditions for an additional 0, 10, or 30 min of chase incubation. The soluble fractions at each chase time point, visualized by BN-PAGE, contained three distinguishable radiolabeled bands, ~180 kD, 550 kD, and 700 kD in size (Figure 2A). The 700-kD region contained all major and minor isoforms of Cpn60, and Cpn60 was its most abundant complex (Figure 2B). The relative abundance of Cpn60 isoforms suggest an $\alpha1_6\beta1_8$ stoichiometry, as reported for Chlamydomonas (Bai et al., 2015; Zhao et al., 2019), with $\alpha2$ and $\beta4$ representing ~0.2 and 0.4% of the total Cpn60, respectively (Supplemental Data Set 2). The intensity of the 700-kD complex decreased with increasing chase time (Figure 2A), consistent with the observed overall decline in Plsp1 detected in the soluble fraction (Figure 2C). The amount of Plsp1 in the membrane fraction increased, and treatment of the membranes with thermolysin showed that Plsp1's degradation product (dp1), which indicates topologically correct integration, also increased over chase time (Figure 2C), consistent with previous results (Endow et al., 2015). The total level of imported Plsp1 stayed consistent throughout the chase, indicating that Plsp1 is not degraded (Figure 2C). The decline in the 700-kD complex therefore correlated with the increased membrane integration (Figure 2D). The behavior of the 700-kD complex is consistent with it serving as an early intermediate in the targeting of Plsp1, as Plsp1 dissociates from Cpn60 prior to its maximal membrane integration.

The 180-kD and 550-kD bands were less prominent than the 700-kD Cpn60 complex (Figure 2A). The 180-kD band did not increase or decrease consistently through the chase

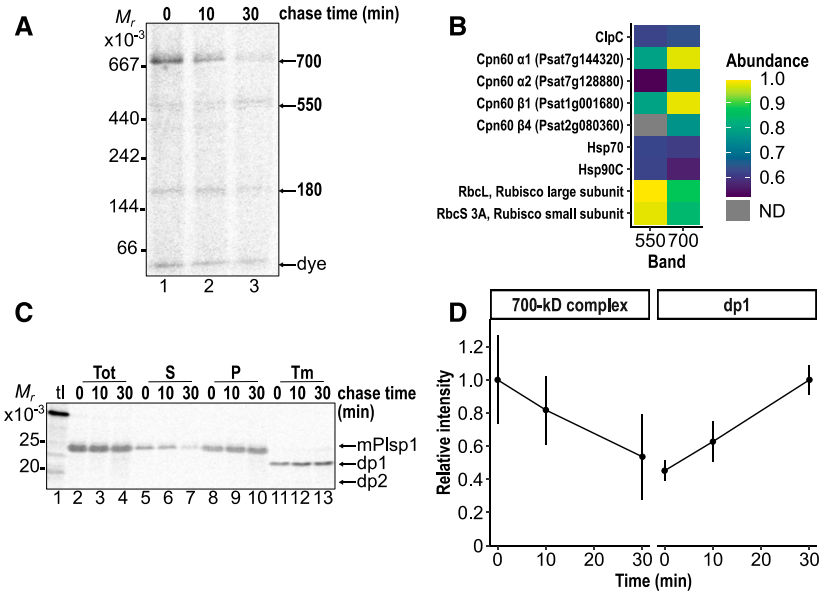

Figure 2. The Level of Plsp1 Interacting with Cpn60 Decreases with Increasing Chase Time.

(A) Import-chase assay followed by BN-PAGE analysis. In vitro-translated, radiolabeled Plsp1 was imported into illuminated (50 $\mu E/m^2s$) chloroplasts with 3 mM ATP for 10 min, followed by treatment with thermolysin for 30 min on ice in the dark to remove unincorporated precursor. The protease was quenched, and intact chloroplasts were reisolated and incubated in the light (50 $\mu E/m^2s$) with 3 mM ATP for 0, 10, or 30 min. Shown is a representative phosphorimage of the equivalent of 6 μg chlorophyll (Chl) of soluble fraction from each chase time-point analyzed by BN-PAGE and autoradiography. Monomeric Plsp1 migrates at the dye front. The distortion that makes the 550-kD band look like a dimer arose from a flaw in the BN-PAGE gel (see Supplemental Figure 2 for a Coomassie-stained image). Import and chase reactions contained 1 mM lincomycin to suppress chloroplast translation of RbcL.

(B) Subset of proteins identified in LC-MS/MS analysis of the 550-kD and 700-kD regions. The 700-kD band was excised from the soluble fraction after a 10-min import; the 550-kD band was excised from the soluble fraction after a 10-min import and a 30-min chase. iBAQ (intensity-based absolute quantification) values from each excised band were normalized to the median to account for variation between band samples. To adjust the scale of the median-normalized abundance values to fall between 0 and 1.0, median-normalized abundance values for each protein were divided by the average median-normalized abundance of RbcL in the 550-kD band (the most abundant protein in any band). Colors indicate relative abundance; gray indicates not detected (ND). Data represent two independent experiments for each band, and independent experiments were performed in triplicate (700-kD) or duplicate (550-kD). For a list of proteins identified, see Supplemental Data Set 2.

(C) Import-chase assay as described in **(A)**, followed by SDS-PAGE analysis of chloroplast subfractions. Representative phosphorimage of the equivalent of 3 μg Chl of total import (Tot), soluble (S), membrane-associated (P), and thermolysin-resistant (Tm) fractions of each chase time point. Equal Chl equivalents were separated on SDS-PAGE alongside 10% input translation (tl). Sizes of mature (M), dp1, and dp2 Plsp1 are indicated.

(D) The intensity of the 700-kD complex at each chase time point was quantified relative to its peak (t = 0 min). The amount of thermolysin-protected dp1 at each chase time point was quantified relative to its peak (t = 30 min). Import-chase assays included in this quantification were performed without lincomycin and analyzed stromal proteins equivalent to 3 μg Chl on both BN-PAGE and SDS-PAGE. Points represent means (n = 10 independent assays for the 700-kD complex; n = 7 independent assays for dp1); error bars are ± 1 SD.

(Supplemental Figure 3) and, as such, was not further characterized. The 550-kD band increased over the course of the chase (Figure 2A; Supplemental Figure 3). The 550-kD region of the gel contained primarily RbcL and RbcS as well as a moderate amount of the major Cpn60 isoforms (Figure 2B). The ribulose-1,5-bisphosphate carboxylase/oxygenase (Rubisco) holoenzyme and the single ring Cpn60 complex observed with isolated oligomers above (Figure 1B) both migrate at this size. The increase in the 550-kD band was largely suppressed when chloroplast translation was inhibited with lincomycin (Supplemental Figures 4A and 4B). Though Plsp1 may contribute to the 550-kD signal, background synthesis of radiolabeled RbcL appears responsible for its increase. These results indicate that the 180-kD and 550-kD bands are not intermediates in Plsp1 targeting.

Cpn60 and cpSec1 Bind Adjacent Plsp1 Sequences

The correlation between increasing membrane association and decreasing Cpn60 interaction suggests that Cpn60 hands Plsp1 off to cpSec1. Our ability to investigate this hypothesis with genetic approaches was limited because Cpn60 is an essential protein (Zhao and Liu, 2018). We therefore determined the Plsp1 domains necessary for interaction with Cpn60 and cpSec1 and the effect of specific stromal factors on integration with in vitro targeting assays.

If Cpn60 binds a specific Plsp1 sequence, we predicted that removing the sequence would impair formation of the 700-kD complex during import. We cloned Plsp1 variants that deleted the TMD, the β strands (β1-2 and β9-10) that are predicted to form the membrane association surface, and the extreme C terminus (Figure 3A; Supplemental Figure 5; Endow et al., 2015; McKinnon et al., 2020). These regions all contain hydrophobic segments likely to bind chaperones. After each deletion construct was imported, we isolated the stroma for BN-PAGE analysis and compared the intensity of the 700-kD complex to a full-length Plsp1 control. We found that Δβ1-2 exhibited a consistent 80% reduction in the intensity of the 700-kD band, indicating that β1-2 is necessary for interaction with Cpn60 (Figures 3B and 3C). In contrast, loss of Plsp1's TMD or C terminus did not alter the 700-kD complex (Figures 3B and 3C). The 550-kD and 180-kD bands were not reduced for any deletion construct (Supplemental Figures 6A and 6B). These results indicate that the β strands immediately adjacent to the TMD are important for the interaction of Plsp1 with Cpn60.

Plsp1 lacks a cleavable thylakoid targeting signal, so cpSec1 must recognize a domain of Plsp1's mature sequence. Deleting that domain may cause defects in targeting, which we visualized by comparing the subfractionation patterns of full-length Plsp1 and the deletion constructs after a 10-min import (Figures 4A and 4E). We quantified how much mature protein, relative to the total imported mature protein, fractionated with soluble proteins (S1), alkaline-extracted peripheral proteins (S2), and alkaline-resistant membrane proteins (P; Figure 4F). Full-length Plsp1 was distributed among S1, S2, and P in a 1:1:2 ratio, with ~18% in S1 (Figure 4A). The ΔTMD construct stalled in the stroma, with 54% found in S1—a threefold increase over full-length Plsp1—and only traces were found associating with the alkaline-resistant pellet (Figure 4B). We previously showed the TMD of Plsp1 was

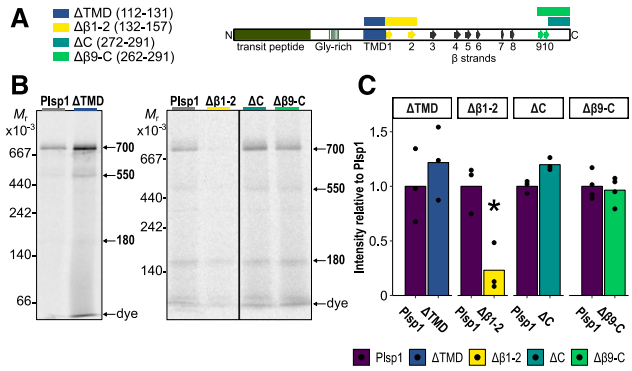

Figure 3. β1-2 Is Necessary for Efficient Interaction with Cpn60.

(A) Structure of full-length Plsp1 with predicted TMD and β strands indicated. β1-2 and β9-10 correspond by homology to the hydrophobic membrane association surface in the *E. coli* leader peptidase crystal structure. Colored bars indicate residues removed for deletion constructs: ΔTMD (112 to 131, blue), Δβ1-2 (132 to 157, yellow), ΔC (272 to 291, teal), and Δβ9-C (262 to 291, green). A homology model showing these regions in the predicted tertiary structure is shown in Supplemental Figure 5.
(B) Import assay followed by BN-PAGE analysis. After a 10-min import of full-length Plsp1 or deletion constructs, intact chloroplasts were lysed hypotonically. The soluble fraction was collected by centrifugation, separated via 4 to 14% BN-PAGE, and visualized by autoradiography. A sample of intact chloroplasts was analyzed directly by SDS-PAGE to confirm import and calculate import efficiency. The black line on gel on the right indicates lanes removed. $n = 3$ for each deletion construct.
(C) To quantify the 700-kD complex, constructs were analyzed pairwise with their full-length Plsp1 controls. Densitometry signals for each deletion construct and the full-length Plsp1 control were normalized to account for different numbers of Met residues and import efficiency. Import efficiency was calculated from an SDS-PAGE phosphorimage that included 10% translation product and a sample of intact chloroplasts. Points represent measurements from at least three independent experiments per construct. Signals from an individual experiment were normalized to the mean of both signals from that experiment; normalized signals for full-length Plsp1 and a deletion construct were then divided by the mean of signals for full-length Plsp1 for all replicates. Significant differences (*$P < 0.05$) between mean full-length and the deletion construct were calculated using a two-sided *t* test with Bonferroni corrections for multiple comparisons (Supplemental Data Set 3).

necessary for cpSec1-dependent integration into isolated thylakoid membranes (Endow et al., 2015). Together, these data indicate that the Plsp1 TMD is its thylakoid targeting signal. Despite altered association with the 700-kD complex, Δβ1-2 distribution among subfractions was indistinguishable from that of full-length Plsp1 (Figure 4C), as was the case for ΔC and Δβ9-C (Figures 4D and 4E). These fractionation patterns indicate all deletions except ΔTMD transit the stroma and reach the thylakoid membrane.

Full integration of Plsp1 into thylakoids results in a characteristic degradation product (dp1) after treatment with the membrane-impermeable protease thermolysin (Figure 4A, lane 6). Neither ΔTMD nor Δβ1-2 yielded such a degradation product after import for 10 min (Figures 4B and 4C, lane 6). An extended 30-min import of Δβ1-2 yielded a faint degradation product that was only ~10% of dp1 from full-length Plsp1 (Supplemental Figure 7). ΔC and Δβ9-C both produced a dp1-equivalent degradation product

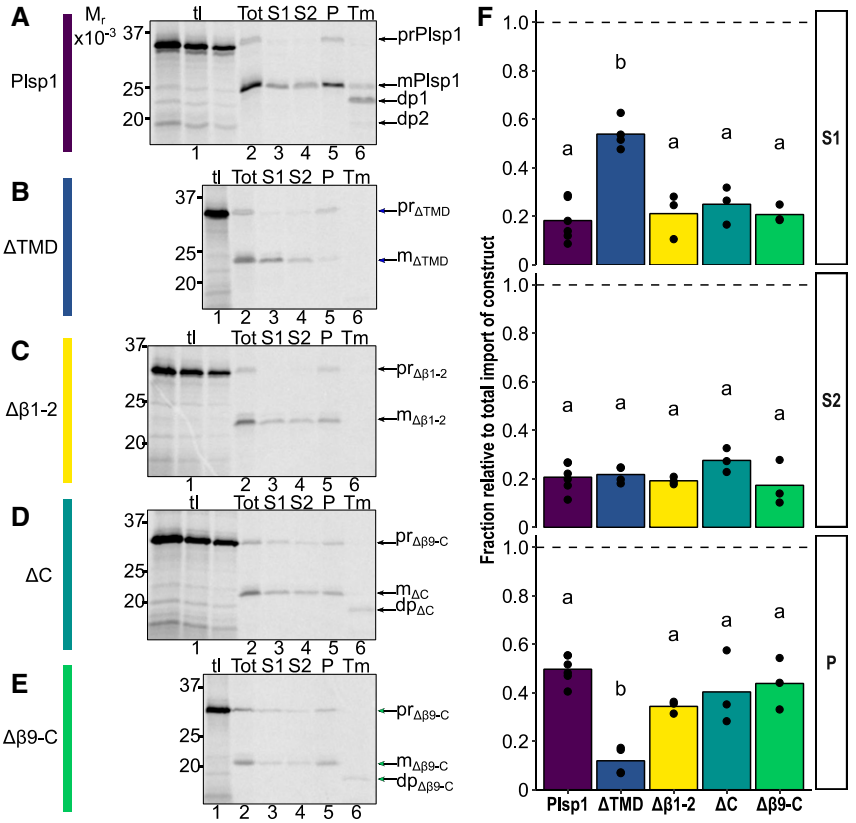

Figure 4. TMD and β1-2 Are Necessary for Membrane Integration.

(A) Subfractionation and integration analysis of full-length Plsp1. After a 10-min import, intact chloroplasts were separated into three samples to analyze total import (Tot), subfractionation, and integration (Tm). The first sample (Tot) was pelleted and analyzed directly. The second sample was lysed hypotonically, and the soluble material (S1) was collected by centrifugation. Membranes were subsequently washed with 0.1 M Na_2CO_3 to extract peripheral membrane proteins. The alkaline-extracted fraction (S2) was separated from the alkaline-resistant membranes (P) by centrifugation. The third sample (Tm) was lysed hypotonically and treated with thermolysin. Equal chlorophyll (Chl) equivalents from each sample were separated on SDS-PAGE alongside 10% translation product (tl). The precursor (pr), mature (M), and thermolysin degradation products of successfully targeted (dp1) and mistargeted (dp2) Plsp1 are indicated.

(B) to **(E)** Analyses as described in **(A)** for ΔTMD **(B)**, Δβ1-2 **(C)**, ΔC **(D)**, and Δβ9-C **(E)**.

(F) The amount of mature protein relative to the total import (Tot) was calculated for S1, S2, and P. Bars represent mean; points represent measurements from at least three independent experiments. Means of the treatments with the same letter do not differ significantly in that fraction based on Tukey HSD for $\alpha = 0.05$; means of the treatments with different letters differ significantly with $P < 0.001$ for all comparisons within that fraction (Supplemental Data Set 3).

(Figures 4D and 4E, lane 6), suggesting that the C terminus of Plsp1 is not necessary for successful insertion. ΔTMD did not associate with the thylakoid membrane (Figure 4B), hence its impeded integration. The inability of Δβ1-2 to bind Cpn60 may result in Δβ1-2 assuming a conformation incompetent for insertion by cpSec1. The β1-2 sequence is also adjacent to the TMD that acts as the thylakoid targeting signal of Plsp1 (Figure 3A), and its deletion may remove part of the sequence that cpSec1 requires to insert Plsp1. The adjacent TMD and β1-2 regions regulate membrane integration. Cpn60 and cpSec1 interact with adjoining sequences of Plsp1.

The Ratio of Cpn60 to cpSecA1 Regulates Plsp1 Integration

With increased mechanistic insight into how Cpn60 and cpSec1 recognize Plsp1, we next asked how Cpn60 and cpSecA1, the extrinsic cpSec1 motor, influenced integration of Plsp1 into isolated thylakoids. Cpn60 and cpSecA1 do not interact in the stroma (Supplemental Figure 8). We previously demonstrated that Plsp1 is integrated by both stromal extract (SE)-independent (Figure 5A, lane 2) and SE-dependent (Figure 5A, lane 3) mechanisms using an in vitro transport assay (Endow et al., 2015). Both mechanisms inserted Plsp1 correctly, resulting in dp1 after thermolysin treatment, and both mechanisms produced in a second degradation product (dp2). Data suggest dp2 represents mistargeted association with the stromal face of the thylakoid (Endow et al., 2015). SE-independent insertion displayed a higher proportion of dp2 (Figure 5A, lane 2), indicating more mistargeting. SE-dependent insertion is mediated by cpSec1 (Endow et al., 2015), and, as previously shown, adding cpSecA1 to the transport assay stimulated dp1 (Figure 5A, lane 4). To test the effect of Cpn60 on integration, we performed the in vitro transport assay in the

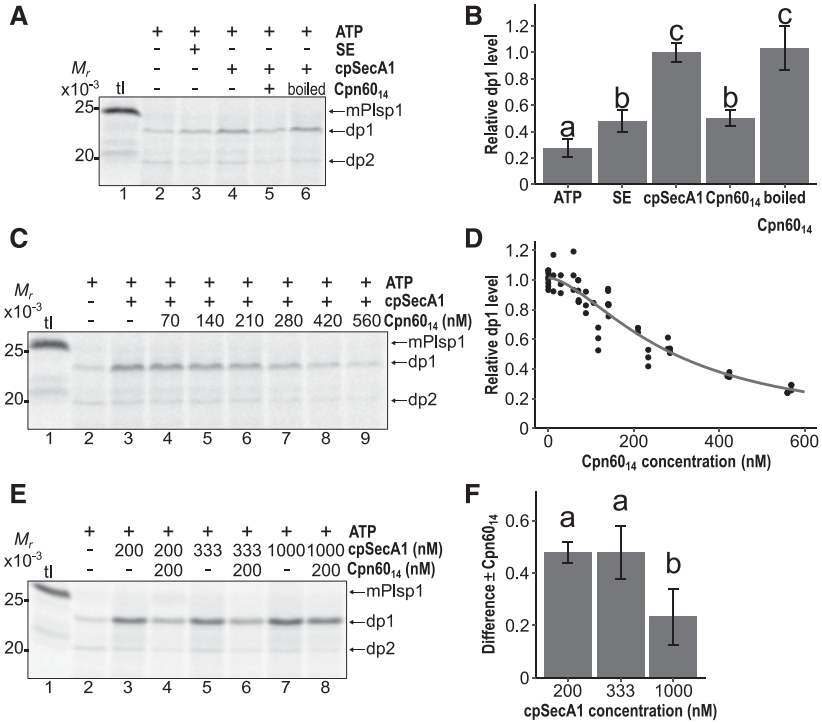

Figure 5. The Balance of Cpn60$_{14}$ to cpSecA1 Influences Integration.

(A) In vitro transport assay. Radiolabeled Plsp1 was incubated with thylakoids in the presence of 5 mM ATP (lanes 2 to 6), SE (lane 3), 200 nM cpSecA1 (lanes 4 to 6), and 200 nM Cpn60$_{14}$ (lane 5; lane 6, boiled) for 30 min in the light (90 μE/m^{2}s). Thylakoids were treated with thermolysin, and equal chlorophyll (Chl) equivalents were separated by SDS-PAGE alongside 5% of the translation product (tl, lane 1) and then visualized by autoradiography. The sizes of mature (mPlsp1) and thermolysin degradation products (dp1, dp2) are indicated. Shown is a representative phosphorimage of three independent experiments performed in triplicate.

(B) Quantification of dp1 from **(A)** relative to dp1 in the presence of ATP and cpSecA1 (A, lane 4). Bars represent means; error bars represent $\pm$ 1 SD. Means of the treatments with the same letter do not differ significantly based on Tukey HSD for $\alpha = 0.05$; means of the treatments with different letters differ significantly with $P < 0.001$ for all comparisons (Supplemental Data Set 3).

(C) In vitro transport assay with different Cpn60$_{14}$ concentrations. Radiolabeled Plsp1 was incubated with thylakoids in the presence of 5 mM ATP (lanes 2 to 9), 200 nM cpSecA1 (lanes 3 to 9), and the indicated concentrations of Cpn60$_{14}$ (lanes 4 to 9) for 30 min in the light (90 μE/m^{2}s). Thylakoids were treated with thermolysin and analyzed as in **(A)**. Shown is a representative phosphorimage of three independent experiments, each in triplicate; exact concentrations of Cpn60$_{14}$ varied between independent experiments.

(D) Quantification of dp1 from **(C)** relative to dp1 in the presence of ATP and cpSecA1 (**C**, lane 3). All replicates are plotted as black points, with a dose-dependence curve (Gadagkar and Call, 2015) fit by least-squares regression to illustrate the relationship between Cpn60$_{14}$ concentration and integration.

(E) In vitro transport assay with different cpSecA1 concentrations. Radiolabeled Plsp1 was incubated with thylakoids in the presence of 5 mM ATP (lanes 2 to 8) and 200 nM (lanes 3 and 4), 333 nM (lanes 5 and 6), or 1000 nM (lanes 7 and 8) cpSecA1 for 30 min in the light (90 μE/m^{2}s). In lanes 4, 6, and 8, 200 nM Cpn60$_{14}$ was included. Thylakoids were treated with thermolysin and analyzed as in **(A)**. Shown is a representative phosphorimage of three independent experiments performed in triplicate.

(F) Quantification of the difference in dp1 **(E)** in the presence and absence of 200 nM Cpn60$_{14}$. dp1 was quantified relative to dp1 in the presence of ATP and 200 nM cpSecA1 (**E**, lane 3), and then the difference between $+$Cpn60$_{14}$ and $-$Cpn60$_{14}$ integration was calculated for each concentration of cpSecA1. Bars represent mean differences; error bars represent $\pm$ 1 SD. Means with the same letter do not differ significantly based on Tukey HSD for $\alpha = 0.05$; means of the treatments with different letters differ significantly with $P < 0.001$ for all comparisons (Supplemental Data Set 3).

presence of equimolar Cpn60$_{14}$ and cpSecA1. These conditions decreased dp1 formation by 50% (Figure 5A, lane 5) compared to the addition of cpSecA1 alone (lane 4). When the added Cpn60 was inactivated by boiling, the level of dp1 did not decrease (Figure 5A, lane 6). Thus, active Cpn60 reduced integration driven by equimolar cpSecA1.

Cpn60$_{14}$ and cpSecA1 are not equimolar in the stroma. We estimated the concentration of Cpn60 α1 and cpSecA1 in SE by immunoblotting with recombinant protein standards (Supplemental Figure 9). With 95% confidence, there were 26 to 37 ng Cpn60 α1 and 6 to 8 ng cpSecA1 per μg stromal protein. The calculated Cpn60$_{14}$ concentration was 24 μM, in rough agreement with the reported concentration of 13 μM (Musgrove et al., 1987). The calculated cpSecA1 concentration was 15 μM. In *E. coli*, it is disputed whether SecA functions as a monomer or dimer (Cranford-Smith and Huber, 2018); in chloroplasts, its migration suggests a dimer (Nakai et al., 1994; Takabayashi et al., 2017). The approximate 3 Cpn60$_{14}$:2 cpSecA1 molar ratio will further vary

based on Cpn60 occupancy and transient local concentration differences. We therefore tested the effect of a range of $Cpn60_{14}$ and cpSecA1 concentrations in the Plsp1 transport assay. At 200 nM cpSecA1, the reduction in dp1 increased as higher concentrations of $Cpn60_{14}$ were added (Figure 5C). Up to 140 nM, $Cpn60_{14}$ had little effect on dp1 production, but 560 nM $Cpn60_{14}$, the maximum added, reduced dp1 production by 77% (Figure 5D). The concentration of $Cpn60_{14}$, which reduced dp1 production by 50%, was calculated to be 290 nM. The reduction was also specific to Cpn60, as equimolar BSA did not affect the level of dp1 (Supplemental Figure 10). While 200 nM $Cpn60_{14}$ reduced dp1 production by 48% at equimolar cpSecA1, the same concentration of $Cpn60_{14}$ only reduced it by only 23% at 1 μM cpSecA1 (Figures 5E and 5F). Increasing cpSecA1 stimulates integration

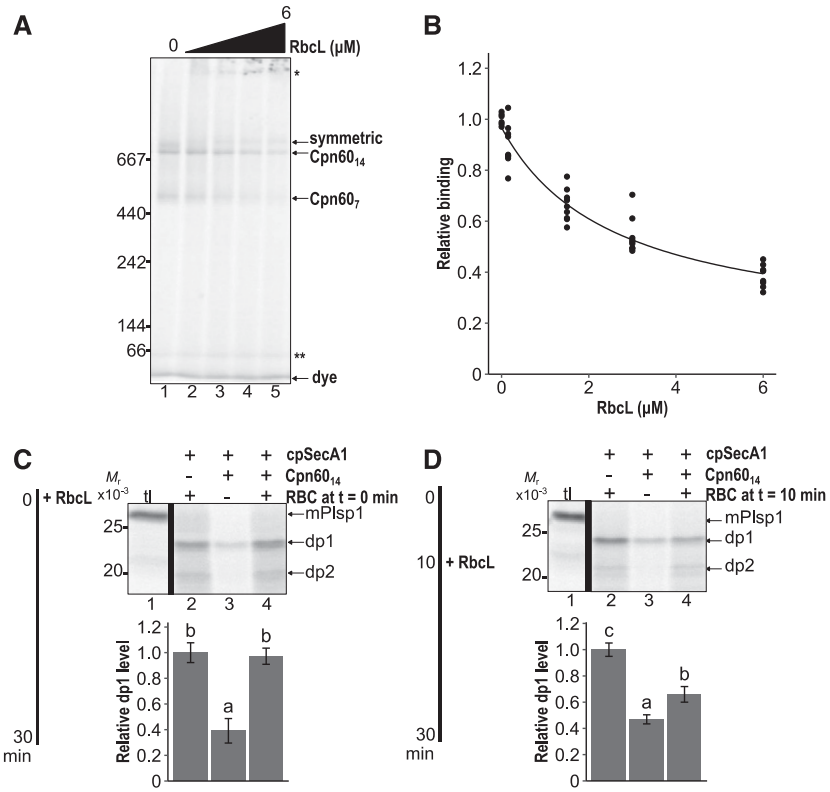

Figure 6. Cpn60-Bound Plsp1 Is Released by Competition with RbcL.

(A) Competition binding assay. In vitro-translated, radiolabeled mPlsp1 was incubated with 200 nM $Cpn60_{14}$ for 5 min at room temperature, then chilled on ice for 5 min before guanidine-denatured RbcL was diluted 36-fold into the reaction. Final concentrations were 0, 0.15, 1.5, 3, or 6 μM RbcL (lanes 1 to 5, respectively). All reactions contained 70 mM guanidine-HCl. Reactions were transferred to room temperature, then analyzed by BN-PAGE and autoradiography. Single asterisks (*) indicate radiolabeled protein that did not enter the BN-PAGE gel; double asterisks (**) indicate free Plsp1. Shown is a representative phosphorimage of three independent experiments performed in triplicate.

(B) The intensity of the $Cpn60_{14}$ band indicated in **(A)** was quantified relative to addition of 0 μM RbcL. Points represent values from independent experiments; the line represents a dose-dependent response curve (Gadagkar and Call, 2015) fit to points.

(C) In vitro transport with RbcL added at t = 0 min. Radiolabeled Plsp1 was mixed with thylakoids in the presence of 5 mM ATP (lanes 2 to 4), 200 nM cpSecA1 (lanes 2 to 4), and, where indicated, 200 nM $Cpn60_{14}$ (lanes 3 and 4) on ice. Black lines mark lanes with an unrelated experiment that were removed. Guanidine-denatured RbcL (lanes 2 and 4) or the equivalent guanidine buffer control were diluted 36-fold into transport reaction (3 μM, final), which was illuminated (90 $\mu E/m^2s$) at room temperature for 30 min. All transport reactions contained 70 mM guanidine-HCl. Thylakoids were treated with thermolysin and analyzed as in Figure 5A. Five percent translation input (tl) and mature, dp1, and dp2 sizes are indicated. dp1 was quantified for each treatment and normalized to transport with cpSecA1 and RbcL (lane 3). Bars represent means; error bars represent ± 1 SD. Means of the treatments with the same letter do not differ significantly based on Tukey HSD for $\alpha = 0.05$; means of the treatments with different letters differ significantly with $P < 0.001$ for all comparisons (Supplemental Data Set 3). $n = 3$ independent experiments, performed in triplicate.

(D) In vitro transport with RbcL added at t = 10 min. Radiolabeled Plsp1 was incubated with thylakoids in the presence of 5 mM ATP (lanes 2 to 4), 200 nM cpSecA1 (lanes 2 to 4), and, where indicated, 200 nM $Cpn60_{14}$ (lanes 3 and 4) for 10 min in the light (90 $\mu E/m^2s$) at room temperature. Black lines mark lanes with an unrelated experiment that were removed. Guanidine-denatured RbcL (lanes 2 and 4) or the equivalent buffer control were diluted 36-fold into transport (3 μM, final) and incubated for 20 min further in the light (90 $\mu E/m^2s$) at room temperature. Thylakoids were treated with thermolysin and analyzed as in Figure 5A. dp1 was quantified and normalized as in **(D)**. Bars represent means; error bars represent ± 1 SD. Means of the treatments with the same letter do not differ significantly based on Tukey HSD for $\alpha = 0.05$; means of the treatments with different letters differ significantly with $P < 0.001$ for all comparisons (Supplemental Data Set 3). $n = 3$ independent experiments, performed in triplicate.

and compensates for the Cpn60-mediated reduction. We conclude that the balance of Cpn60 to cpSecA1 is a key regulator of the extent to which Plsp1 is integrated.

Plsp1 Displaced from Cpn60 Is Accessible to cpSec1

To exchange Plsp1 between Cpn60 and cpSec1, Plsp1 must ultimately dissociate from Cpn60. Nonnative substrates can rapidly rebind chaperonins after release; however, substrates with higher dependence on chaperonins for folding will outcompete less-stringent substrates (Kerner et al., 2005). To determine if Cpn60-bound Plsp1 releases and rebinds, we prebound radiolabeled mature Plsp1 to Cpn60, then added an excess of chemically denatured Rubisco as a competitor (Figure 6A). RbcL exhibits obligate dependence on Cpn60 for folding (Aigner et al., 2017). Higher concentrations of RbcL increasingly displaced the radiolabeled Plsp1 from binding Cpn60 (Figure 6A). The maximum RbcL added, a 30-fold molar excess over $Cpn60_{14}$, reduced the binding of Plsp1 to 38% of the mock RbcL addition (Figure 6B). Free Plsp1 did not increase at the high concentrations of added RbcL (Figure 6A, indicated by **), but instead, more radiolabeled protein failed to enter the gel entirely (Figure 6A, indicated by *). During these experiments, a minor proportion of Cpn60 migrated slightly above the 700-kD $Cpn60_{14}$ band, which we attribute to substrate occupying both rings in a symmetrical complex like those observed for GroEL and Hsp60 (Figure 6A; Weiss et al., 2016; Bigman and Horovitz, 2019). From this experiment, we conclude that nonnative RbcL can outcompete Plsp1 from rebinding Cpn60.

The release of Plsp1 from Cpn60 should allow its recognition by cpSec1 for membrane integration (Figure 6A). We tested if the addition of RbcL during the in vitro Plsp1 transport assay alleviated the competition by Cpn60. Plsp1 integration proceeds linearly for ~10 min then continues to slowly increase during a 30-min transport. We added 3 μM denatured RbcL either at t = 0 min to initiate the assay (Figure 6C) or at t = 10 min into the Plsp1 transport reaction (Figure 6D). When RbcL was added to transport reactions at t = 0 min, the amount of dp1 ultimately produced was the same in the presence or absence of Cpn60 (Figure 6C, compare lanes 3 and 5). The integration of Plsp1 was fully restored by competitive RbcL. When RbcL was added to transport reactions at t = 10 min, the amount of dp1 in the presence of Cpn60 increased but did not fully recover to the level of the control (Figure 6D). RbcL displacement was less effective at room temperature than on ice (Figure 6B; Supplemental Figure 11), which might partially account for the incomplete restoration of integration. From these results, we conclude that Plsp1 released from Cpn60 is accessible to cpSec1.

When cpSRP43 or cytosolic Hsp70 provide chaperone assistance to membrane-targeted substrates, they actively maintain their substrates in an unfolded, insertion-competent conformation (Payan and Cline, 1991; Jaru-Ampornpan et al., 2010; Cho and Shan, 2018). We modified an assay used to demonstrate that SE maintained the transport competence of LHCP over 1 h of pretreatment in order to test the effect of stromal chaperones and Cpn60 on the ability of Plsp1 to integrate (Payan and Cline, 1991). In our experiments, pretreatment of in vitro translated Plsp1 with buffer, SE, or $Cpn60_{14}$ occurred for 0, 10, 30, or 60 min (Figures 7A and 7B). After 60 min, only 68% of buffer-pretreated Plsp1 remained transport competent (Figure 7B). Incubation with either SE or $Cpn60_{14}$ did not provide detectable enhancement to transport competence at any time point tested (Figures 7A and 7B). In summary, although Plsp1 interacts with Cpn60 in the stroma, this interaction cannot protect Plsp1 from losing its ability to integrate over time.

DISCUSSION

Approximately 90% of thylakoid TM proteins transit the aqueous stroma prior to integration, assisted by largely unidentified mechanisms. The nuclear-encoded Plsp1 binds to Cpn60, as demonstrated by in vitro pulldown, reconstitution, and proteinase K protection assays (Figure 1). Plsp1 pulls down the abundant Cpn60 α1 and β1 isoforms, but not the substrate-specialized α2 or β4 isoforms (Peng et al., 2011; Ke et al., 2017), indicating that Plsp1 is a substrate of the major housekeeping Cpn60 oligomer. Involvement of Cpn60 in cpSec1-mediated targeting was unexpected, considering its classical role as a folding chaperone in cooperation with Cpn10, Cpn20, and ATP. Chaperonins bind and encapsulate proteins, typically favoring their substrate's assumption of its native conformation, though this often requires multiple cycles of encapsulation (Hayer-Hartl et al., 2016). The increased integration resulting from RbcL displacing Plsp1 from

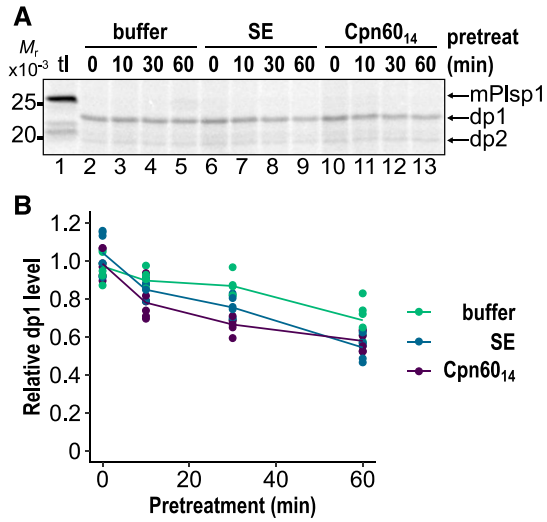

Figure 7. Neither Cpn60 nor Other Stromal Chaperones Actively Maintain Plsp1's Transport Competence.

(A) In vitro translated, radiolabeled Plsp1 was pretreated with buffer, SE, or 200 nM $Cpn60_{14}$ for 0, 10, 30, or 60 min at room temperature. Pretreatments were adjusted such that all reactions contained final concentrations of 40 nM $Cpn60_{14}$ and 0.2 mg/mL chlorophyll equivalent SE, then incubated with thylakoids in the presence of 5 mM ATP and 200 nM cpSecA1 for 30 min in the light (90 $\mu E/m^2s$). Thylakoids were treated with thermolysin and analyzed by SDS-PAGE alongside 5% of the input translation product (tl). Shown is a representative phosphorimage of three independent experiments performed in duplicate.

(B) Quantification of dp1 from **(A)** relative to the mean of all t = 0 min pretreatment samples (lanes 2, 6, and 10). Points are all replicates, colored by treatment; lines are drawn to assist visualization.

Cpn60 (Figures 6D and 6E) suggests that Cpn60-bound Plsp1 retains a nonnative confirmation. Cpn60 interacts with the Plsp1 sequences, which will fold to form its hydrophobic membrane association surface (Figures 3B and 3C). Because lipid association is critical for folding catalytically active Plsp1 (McKinnon et al., 2020), it may be unfavorable for Plsp1 to fold within the chaperonin. Unfolded Plsp1 bound by a Cpn60 $\alpha1\beta1$ oligomer would remain competent for thylakoid insertion.

Our in vitro targeting assays in isolated thylakoids (Figures 5 and 6) and intact chloroplasts (Figure 2) support Cpn60 holding Plsp1 transiently prior to its thylakoid insertion. Three models could explain the hand-off of Plsp1 from Cpn60 to cpSec1 (Supplemental Figure 12). First, Cpn60 could bind to cpSec1 components and pass Plsp1 to the translocon. In this model, Cpn60 functions analogously to cpSRP or SecB, the *E. coli* targeting factor which delivers unfolded secreted proteins but which is not conserved in chloroplasts (Dempsey et al., 2004; Sala et al., 2014). We did not detect interaction between cpSecA1 and Cpn60 in the stroma in the absence of Plsp1 (Supplemental Figure 8), though we cannot exclude Plsp1-mediated interaction between these proteins. If Cpn60 behaved like cpSRP or SecB, we would expect Cpn60 to stimulate integration of Plsp1, and this is inconsistent with our in vitro transport assay results (Figure 5).

Second, Cpn60 could pass Plsp1 to another stromal factor in order for this additional component to deliver Plsp1 to cpSec1. There were no other clear candidates identified in the pulldown assay (Figure 1; Table 1), though the pulldown assay would not detect proteins that interacted solely with the TMD of Plsp1. The known additional stromal protein involved in targeting Plsp1 is cpSecA1. However, while cpSecA1 interacts with its substrates at the thylakoid membrane, cpSecA1 has not been detected binding its substrates in the stroma to recruit them to the membrane (Haward et al., 1997; Ma, 2000). We did not identify another stromal protein in our pulldown (Figure 1) or complex in our import-chase assays (Figure 2) that appeared to act as an intermediate between Cpn60 and cpSec1. These two models are not supported well by our data.

The third potential hand-off mechanism is a catch-and-release model in which Plsp1 cycles on and off Cpn60, rebinding Cpn60 until encountering cpSec1. During in vitro transport in isolated thylakoids, Cpn60 reduced Plsp1 integration (Figure 5). ATP hydrolysis and displacement by RbcL released Plsp1 from Cpn60 for insertion into the thylakoid (Figure 6). The effect of RbcL can be attributed to two processes, which are not mutually exclusive. First, occupying Cpn60 with RbcL lowers the apparent concentration of free Cpn60 to bind Plsp1. Second, given that chaperonins preferentially bind obligate substrates like RbcL over less stringent substrates (Kerner et al., 2005), RbcL will outcompete Plsp1 and more readily rebind Cpn60 during chaperonin cycling. Increasing cpSecA1 also partially restored integration (Figures 5E and 5F), suggesting that Plsp1 exists in an equilibrium between Cpn60- and cpSecA1-bound forms. The correlation between reduced Cpn60 interaction and increased dp1 during import-chase experiments (Figure 2C) implies that, ultimately, cpSecA1 collects the imported Plsp1 recently released from Cpn60. Our data best support the catch-and-release model in which Cpn60 captures and releases Plsp1 cyclically, while cpSec1 recognizes free stromal Plsp1 and integrates it. The cpSec1 translocon depletes the free Plsp1 from the stroma, and by mass action, Cpn60 continuously releases its Plsp1 population until integration is complete.

Efficient hand-off of Plsp1 to cpSec1 was influenced by displacement of Plsp1 from Cpn60 by other chaperonin substrates. Our in vitro binding and transport assays used RbcL because it is firmly established as a substrate specifically requiring Cpn60 for proper folding. In our second-dimension analysis, we observed RbcL corresponding to ~20% of the assembled RbcL pool comigrating with Cpn60 (Supplemental Figure 4B), consistent with other reports (Peltier et al., 2006; Olinares et al., 2010; Feiz et al., 2012, 2014), and RbcL was abundant in our excised 700-kD Cpn60 complex (Figure 2). We also detected minor levels of other known Cpn60 substrates comigrating with the 700-kD complex: NdhH (Peng et al., 2011), CF1-α, CF1-β (Chen and Jagendorf, 1994; Mao et al., 2015), and Gln synthetase (Lubben et al., 1989; Supplemental Data Set 2). In *E. coli*, experiments suggest that 99% of available chaperonins are occupied by substrates (Kerner et al., 2005; Jewett and Shea, 2010). Our data are likewise consistent with a heavily occupied Cpn60.

For RbcL, its physiological concentrations are not dissimilar to the molar excess of chemically denatured RbcL that we added in vitro. The steady-state concentration of active RbcL in chloroplasts was measured at ~4 mM (Jensen and Bahr, 1977). In slowly growing Arabidopsis (*Arabidopsis thaliana*) leaves, 3% of the RbcL pool was replaced each day; in rapidly growing Arabidopsis leaves, the fraction of newly synthesized RbcL increased to 35% each day (Li et al., 2017). Assuming 13 μM Cpn60 in the chloroplast (Musgrove et al., 1987), each Cpn60 must fold 0.4 to 5 RbcL per hour. Estimated rates of RbcL folding by chaperonins (~0.2 min^{-1}, Viitanen et al., 1995; Liu et al., 2010; Hauser et al., 2015) suggest that newly synthesized RbcL will occupy 3 to 40% of the capacity of a single Cpn60 per hour, depending on growth rates. The targeting of Plsp1 is likely highest in growing leaves (Schmid et al., 2005; Hsu et al., 2011) that also have high RbcL synthesis rates (Lorimer, 1996; Li et al., 2017). Additionally, it has been clear from the first report of an RbcL interaction with Cpn60 (Barraclough and Ellis, 1980) that Rubisco holoenzyme assembly, not RbcL synthesis, is rate limiting. Rubisco assembly requires Cpn60 to fold RbcL, then four other chaperones to construct the $RbcL_8$-$RbcS_8$ complex, and the in vivo kinetics of this process remain opaque (Vitlin Gruber and Feiz, 2018). If the assembly chaperones are unavailable, RbcL remains bound to Cpn60 (Feiz et al., 2012, 2014). There is clearly enough Cpn60 free to interact with Plsp1 in the stroma, but sufficiently high concentrations of RbcL and other endogenous substrates are present to displace Plsp1 from Cpn60.

Does Cpn60 serve as a simple waystation, or does it actively maintain Plsp1's transport competence? Our data present a complex picture. Biochemical and genetic evidence suggests a limited role for GroEL in stabilizing transport-competent states of secreted proteins (Kusukawa et al., 1989; Lecker et al., 1989; Van Dyk et al., 1989; Brundage et al., 1990; Phillips and Silhavy, 1990; Danese et al., 1995; Kerner et al., 2005; Pradel et al., 2009; Castanié-Cornet et al., 2014) and in stabilizing membrane proteins in vitro (Bochkareva et al., 1996; Deaton et al., 2004). Although cpSRP43 can prevent LHCP aggregation and rescue aggregated LHCP, maintaining complete transport competence over 1 h of

room temperature pretreatment (Payan and Cline, 1991; Jaru-Ampornpan et al., 2010), we were unable to detect any stromal protein, including Cpn60, that performed this function for Plsp1 (Figure 7). If Plsp1 remains bound to Cpn60 but loses its insertion competence, Cpn60 may be able to reroute Plsp1 to a quality-control pathway through its interaction with FtsH11 (Adam et al., 2019). Maintenance of competence by Cpn60 may be detected under more stressful in vitro conditions (for example, higher temperature), although in chloroplasts experiencing such stress, the number of stromal proteins interacting with Cpn60 would increase, reducing its ability to protect Plsp1 in particular. However, when Plsp1 loses the ability to interact with Cpn60 through its hydrophobic membrane association surface (β1-2) or with cpSec1 through its thylakoid targeting signal (TMD), its thylakoid integration is abolished (Figure 4). Δβ1-2 Plsp1 fractionates with membranes (Figure 4B), and its failure to integrate suggests that it assumes a transport-incompetent conformation, although it is also possible that this deletion compromises the targeting signal. Cpn60 interaction is not necessary for Plsp1 to integrate in vitro, nor does it extend the transport competence of Plsp1 in vitro. However, in intact chloroplasts, losing Cpn60 interaction correlates with compromised integration.

Cpn60 is essential, and this precluded the use of genetic knockout approaches to study the importance of Cpn60 for Plsp1 targeting. Cpn60 α1 mutants exhibit embryo lethality in Arabidopsis and seedling lethality in maize (*Zea mays*; Barkan, 1993; Feiz et al., 2012) and rice (*Oryza sativa*; Kim et al., 2013). Double mutants of redundant β1 isoforms in Arabidopsis result in seedling lethality (Suzuki et al., 2009; Ke et al., 2017). Mild Cpn60 β1 knockdown in tobacco (*Nicotiana tabacum*) causes leaf chlorosis and starch accumulation in chloroplasts, suggesting that chloroplast development is perturbed (Zabaleta et al., 1994). In principle, inducible Cpn60 knockdown mutants could be generated to examine the effect on Plsp1's targeting and on thylakoid development in general, but such study is outside the scope of this work. Mutants with impaired chloroplast proteostasis, including those disrupting the cpSRP pathway, often show increased accumulation of Cpn60 and other chaperones to compensate (Rutschow et al., 2008; Nishimura and van Wijk, 2015). While Cpn60 is not the only chaperone available to assist thylakoid TM protein targeting, Cpn60 provides a possible path for proteins transiting the stroma.

In summary, our results demonstrate interaction between Plsp1 and Cpn60 and support a mechanism by which Cpn60 holds Plsp1 until the cpSec1 translocon recruits it to the membrane for integration.

METHODS

DNA Constructs

Plasmids encoding prPlsp1 and mPlsp1 for in vitro translation (Endow et al., 2015) and mOE33 (Chou et al., 2006) and cpSecA1 (Endow et al., 2015) for recombinant expression in *Escherichia coli* were described previously. To generate the internal prPlsp1 deletions ΔTMD (residues 112 to 131) and Δβ1-2 (132 to n157), two fragments were amplified from prPlsp1 in pIVTGW-SP6 with the indicated primers (Supplemental Table 1) and were then combined by long-flanking homology PCR (Tian et al., 2004; Endow et al., 2015). To generate C-terminal prPlsp1 deletions ΔC (272 to 291) and Δβ9-C (262 to 291), prPlsp1 was amplified using the indicated primers complementary to the new 5′ end. Plsp1 deletion constructs were subcloned into pIVTGW-SP6 (Endow et al., 2015) by Gateway cloning for in vitro translation. mPlsp1$_{\Delta TMD}$ was amplified from prPlsp1$_{\Delta TMD}$ in pIVTGW-SP6 with primers containing *Nde*I and *Bam*HI restriction sites, digested, and ligated into similarly digested pET16b (Novagen). Untagged *Pisum sativum* Cpn60α1 (Psat7g144320) and Cpn60β1 (Psat1g001680) constructs were a gift from Abdussalam Azem (Dickson et al., 2000). To add purification tags, Cpn60α1 in pET24a (Dickson et al., 2000) was excised with *Nde*I and *Bam*HI then ligated into similarly digested pET16b. Cpn60β1 was amplified from pET24d (Dickson et al., 2000) with primers adding a 5′-*Nde*I and 3′-*Xho*I site and cloned into pCR2.1 using an Invitrogen TOPO-TA kit. Cpn60β1 was digested with *Nde*I and *Xho*I, then ligated into similarly digested pET16b.

Protein Preparation

For radiolabeled proteins, constructs were translated in vitro using a TNT coupled rabbit reticulocyte lysate kit (Promega). His-mPlsp1$_{\Delta TMD}$, His-mOE33 (Chou et al., 2006), His-Cpn60 α1, His-Cpn60 β1, and His-cpSecA1 (Endow et al., 2015) were expressed in *E. coli* and purified by nickel-nitrilotriacetic acid (Ni-NTA) affinity chromatography. Full expression and purification details may be found in the Supplemental Methods. Protein purity was assessed by SDS-PAGE and concentration by Bradford assay (Bio-Rad).

Isolation of Chloroplasts, Thylakoids, and Concentrated SE

Intact chloroplasts were isolated from 9- to 13-d-old *P. sativum* seedlings as described by Inoue and Keegstra (2003). In brief, pea tissue was homogenized in cold grinding buffer (50 mM HEPES-KOH, pH 7.3, 330 mM sorbitol, 1 mM $MgCl_2$, 1 mM $MnCl_2$, 2 mM EDTA, 0.1% [w/v] BSA), filtered through two layers of Miracloth, and centrifuged at 3000*g*, 4°C for 5 min. The pellet was resuspended in cold grinding buffer and layered on a continuous Percoll gradient and centrifuged at 8000*g*, 4°C for 10 min. The intact chloroplast band was recovered and washed twice with import buffer (IB; 50 mM HEPES-KOH, pH 8.0, 330 mM sorbitol). Preparation of thylakoids and concentrated SE (at 2.5 mg chlorophyll equivalent chloroplasts/mL) was as described by Endow et al. (2015) and Asher et al. (2018). In brief, pelleted intact chloroplasts were resuspended to 1 mg/mL chlorophyll in 10 mM HEPES-KOH, pH 8.0, 10 mM $MgCl_2$ (HM) and incubated on ice in the dark for 10 min. Thylakoids were separated from stromal proteins by centrifugation at 3200*g*, 4°C for 8 min. The thylakoid pellet was suspended in two volumes of HM, centrifuged at 3200*g*, 4°C, and resuspended to 1 mg/mL chlorophyll in 50 mM HEPES-KOH, pH 8.0, 330 mM sorbitol, 10 mM $MgCl_2$ (IBM). The stromal supernatant was clarified of residual membranes at 42,000*g*, 4°C for 30 min. Ninety-five percent of the supernatant was recovered and concentrated using an Amicon Ultra-4 30000NMWL filter (EMD Millipore).

In Vitro Pulldown Assay

In vitro pulldown was modified from studies by Flores-Pérez et al. (2016) and Peng et al. (2011). One hundred microliters SE was mixed with 20 μg of recombinant protein in binding buffer: 50 mM HEPES, pH 8.0, 3.3 mM Tris, 330 mM sorbitol, 20 mM imidazole, 13.3 mM NaCl, 10 mM $MgCl_2$, 10 mM ADP, 20 mM Glc, and 20 U/mL hexokinase (Roche). The sample was incubated with rocking at 4°C for 1 h then added to 20 μL Ni-NTA equilibrated with binding buffer without ADP, Glc, or hexokinase. Proteins were bound to Ni-NTA overnight at 4°C with rotation. The solution was transferred to a 200-μL column (Promega). Unbound proteins were collected by centrifugation at 800*g* for 1 min, then the resin was washed with 3 mL of SE

buffer: 50 mM HEPES, pH 8.0, 330 mM sorbitol, 10 mM $MgCl_2^-$, and 20 mM imidazole. For sequential elution, the resin was incubated with 60 μL of 10 mM Mg-ATP or 60 μL 300 mM imidazole in 50 mM HEPES, pH 8.0, 330 mM sorbitol, 10 mM $MgCl_2$ for 5 min before centrifugation. Aliquots were analyzed by 12% SDS-PAGE and immunoblotting. For liquid chromatography-tandem mass spectrometry (LC-MS/MS) analysis, 50% of the first imidazole elution was separated via SDS-PAGE, stained, and excised.

In Vitro Chaperonin Oligomer Reconstitution Assay

In vitro reconstitution was performed as described by Dickson et al. (2000), Vitlin et al. (2011), and Vitlin Gruber et al. (2014): 50 μM Cpn60 α1 and β1 and 25 μM Cpn20 were incubated in 50 mM Tris-HCl, pH 8.0, 300 mM NaCl, 10 mM $MgCl_2$, 4 mM KCl, 2 mM DTT, and 1.6 mM MgATP at room temperature for 5 min, then at 30°C for 1 h. To separate tetradecameric ($Cpn60_{14}$) Cpn60 from other oligomers, the reconstitution reaction was separated by size-exclusion chromatography on a GE Superose 6 column in 50 mM HEPES-KOH, pH 8.0, 100 mM NaCl, 5% (v/v) glycerol at room temperature. The oligomeric state was confirmed by separating 5-μL equivalents of fractions on 6% native-PAGE. Fractions containing $Cpn60_{14}$ were pooled and concentrated in an Amicon 30K MWCO filter. Concentrated $Cpn60_{14}$ was quantified by Bradford assay (Bio-Rad). The calculated molecular weights of His-tagged Cpn60α and Cpn60β monomers were used to calculate the molecular weight of an α7β7 oligomer, and concentrations are presented in terms of oligomer unless otherwise stated.

In Vitro Chaperonin Binding

Chaperonin binding assay reactions included 200 nM $Cpn60_{14}$ and 5% (v/v) radiolabeled mPlsp1 in 50 mM HEPES-KOH, pH 8.0, 330 mM sorbitol (IB). For experiments in Figure 1B, reactions were incubated for 30 min at room temperature. Addition of 10 mM MgATP or AMP-PNP was followed by incubation for 10 min at room temperature. Five microliters of the binding reaction was separated by 4 to 14% BN-PAGE, as described by Endow and Inoue (2013).

Proteinase K Protection Time Course

Proteinase K protection time courses were performed at room temperature as described by Mao et al. (2015) with modifications. Treatments were (1) $Cpn60_{14}$, (2) $Cpn60_{14}$ and Cpn20, (3) Cpn20, (4) BSA and Cpn20, or (5) buffer only (no addition). Radiolabeled Plsp1, produced by in vitro translation, was incubated with $Cpn60_{14}$, BSA, or buffer for 30 min. ADP was added to all treatments, and Cpn20 was added to designated treatments, followed by a 10-min incubation. The protease protection assay was initiated by the addition of 1.2 μg/mL proteinase K (Sigma-Aldrich P2308). Aliquots were removed at 0, 10, 20, and 60 min and immediately quenched by addition of 1 mM phenylmethylsulfonyl fluoride in isopropanol. Final concentrations of components were 2% (v/v) substrate, 0.8 μM $Cpn60_{14}$, 2 μM Cpn20, 11.2 μM BSA (equivalent to $Cpn60_{14}$ in terms of monomer), and 1 mM ADP in proteinase K buffer (50 mM Tris-HCl, pH 7.5, 50 mM KCl, 5 mM $MgCl_2$).

The samples were separated on 12% SDS-PAGE alongside 100% and 50% substrate input standards. Radioactive signals were quantified by densitometry in ImageJ (Schneider, Rasband, and Eliceiri, 2012). The protected fraction was calculated for each treatment, normalized to the mean of the 0-min time points per treatment. Data were fit to a falling single exponential by least-squares regression in Kaleidograph (Synergy Software, version 4.1.1).

In Vitro Protein Import

Protein import assays with intact chloroplasts were performed as described by Inoue and Keegstra (2003). In brief, reactions containing chloroplasts at 0.25 mg/mL chlorophyll (Chl), 3 mM MgATP, and 10% translation in IB were incubated in the light (20 to 40 μE/m^2s). Intact chloroplasts were reisolated through 40% (v/v) Percoll in IB. An aliquot of each import was used to quantify chloroplast recovery; the remainder was pelleted at 2000*g* and either used for subsequent analysis or resuspended to 0.3 mg/mL Chl in SDS-PAGE sample buffer.

The import-chase assay was performed as described, with minor modifications, by Endow et al. (2015). One millimolar lincomycin was included throughout import and chase in a subset of experiments to suppress chloroplast translation (Kim et al., 1994; Chotewutmontri and Barkan, 2018). After a 10-min import assay, chloroplasts were diluted in ice-cold IB to less than or equal to 0.5 mM ATP, pelleted, and treated with 0.2 μg/μL thermolysin to remove unincorporated precursor. Thermolysin activity was quenched with 10 mM EDTA, and intact chloroplasts were recovered through 40% (v/v) Percoll, washed, and divided into three equal aliquots. Three millimolar ATP addition initiated the chase, with chase incubations in light staggered to end simultaneously. An aliquot (~4 μg Chl) of intact chloroplasts from each chase was reserved as total import (T), and the remainder was lysed in 10 mM HEPES-KOH, pH 8.0, 10 mM $MgCl_2$ (HM) at 1 mg/mL initial Chl for 10 min on ice. The soluble fraction was collected by centrifugation at 16,000*g* for 20 min and clarified of any residual membranes in a second 16,000*g*, 20-min centrifugation. The pellet was treated with 0.1 μg/uL thermolysin for 40 min on ice. For the experiments quantified in Figure 2C, the supernatant was adjusted so that 3 μg Chl was analyzed by 4 to 14% BN-PAGE. For BN-PAGE, the supernatant was mixed with two volumes of BN-PAGE loading solution.

Fractionation into soluble (S1), alkaline-extracted (S2), and alkaline-resistant (P) samples was as described by Inoue et al. (2006). In brief, chloroplasts were lysed in HM and the soluble (S1) fraction was collected by centrifugation at 16,000*g* for 20 min. The pellet was washed in 0.1 M Na_2CO_3 for 10 min on ice, and the alkaline-extracted (S2) fraction collected by centrifugation at 16,000*g* for 20 min. The pellet (P) represented alkaline-resistant proteins. When soluble complexes were analyzed by BN-PAGE (Figure 3), reisolated chloroplasts were lysed in HM at 1 mg/mL initial Chl concentration. As described for import-chase assays, the soluble fraction after centrifugation was spun for a further 20 min at 16,000*g* to pellet any residual membranes.

In Vitro Transport

Protein transport assays with isolated thylakoids were performed as described by Endow et al. (2015) and Asher et al. (2018). In brief, reactions contained thylakoids at 0.33 mg/mL Chl, 5 mM MgATP, and 10% translation product and were incubated at room temperature for 30 min in the light (70 to 100 μE/m^2s). Integration was assessed by treatment with 0.1 μg/μL thermolysin for 40 min on ice. After thermolysin activity was quenched with EDTA, recovered membrane pellets were analyzed by SDS-PAGE. When cpSecA1, Cpn60 $Cpn60_{14}$, or Rubisco were included, control reactions were supplemented with their respective buffers.

Rubisco Displacement Assays

Spinach Rubisco (Sigma-Aldrich R8000, $RbcL_8$:$Rbcs_8$) was denatured in 6M guanidine-HCl, 5 mM DTT for 30 min at room temperature. RbcL and RbcS were quantified by densitometry relative to BSA, and the calculated concentration of RbcL was reported. Whenever RbcL was added, an equal concentration of denatured RbcS was also present. The final concentration of guanidine-HCl in binding and transport assays was 70 mM, which did not inhibit Cpn60-Plsp1 binding and inhibited transport by 20%. To minimize guanidine-HCl addition, denatured RbcL was diluted to 2.5 M guanidine-

HCl immediately before its addition to binding or transport assays. Six micromolar RbcL was the highest final concentration that could be added without immediate aggregation.

For RbcL displacement analysis in chaperonin binding assays, conditions were modified from a study by Liu et al. (2010). Reactions contained 200 nM Cpn60 $Cpn60_{14}$, 5 mM DTT, 1 mg/mL BSA, and 5% (v/v) radiolabeled mPlsp1. Reactions were incubated at room temperature for 5 min, then chilled on ice for 5 min. Denatured RbcL was diluted 36-fold into the chilled reaction, which was transferred back to room temperature for 20 min. Five microliters of the binding reaction was analyzed by 4 to 14% BN-PAGE. Each independent experiment was performed in triplicate for each RbcL concentration and in duplicate for mock buffer addition.

To analyze the effect of RbcL on in vitro transport, denatured RbcL was diluted 36-fold to 3 μM at t = 0 or t = 10 min of a 30-min transport assay. When RbcL was added at t = 0 min, it was the last component added to an ice-cold transport reaction before the reaction was transferred to light at room temperature; when RbcL was added at t = 10 min, the transport reaction was equilibrated to room temperature.

LC-MS/MS and Data Analysis

In-gel trypsin digestion and LC-MS/MS were performed at the University of California, Davis Proteomics Core Facility. Peptide identification and label-free quantification (LFQ ratio equal to 1) were performed in MaxQuant (1.5.6.0) using default parameters (Cox and Mann, 2008). Full details describing generation of a *P. sativum* search database and data processing and analysis may be found in the Supplemental Methods.

Stromal Concentration of $Cpn60_{14}$ and cpSecA1 Estimation

The crude approximation of the stromal concentration of $Cpn60_{14}$ and cpSecA1 were based on a method used to approximate RbcL concentrations (Jensen and Bahr, 1977). The estimated μL stroma per mg Chl volume used were 20, 25, or 40 μL per mg Chl (Heldt, 1980; Howitz and McCarty, 1982; Robinson, 1984). The molecular weight of mature cpSecA1 and Cpn60α1 was predicted by Expasy. The $Cpn60_{14}$ oligomer calculation assumed that the stromal oligomer contains 6 Cpn60α1 protomers, consistent with our data (Supplemental Data Set 2) and LC-MS/MS-based approximations in *Chlamydomonas* (Bai et al., 2015; Zhao et al., 2019).

Antibodies

Antibodies used in this work were anti-Hsp60 (1:10,000, Enzo, SPA-807 lot 08,041,418), anti-His (1:5000, Santa Cruz, SC-803 lot G2506), anti-OE33 (Chou et al., 2006), anti-cpSecA (Nakai et al., 1994), and anti-Cpn60α1 (1:5000, Agrisera, AS12 2613 lot 1309).

Nomenclature

In this study, we refer to Cpn60 isoforms according to the convention used by TAIR for Arabidopsis that orders isoforms by expression level. Supplemental Table 2 lists the *P. sativum* (Psat) gene identifiers (v1a; Kreplak et al., 2019), *P. sativum* UniProt identifiers, and corresponding Arabidopsis gene identifiers (Araport 11) for each Cpn60 isoform.

Accession Numbers

Protein sequences for the purified proteins used in this article can be found in the GenBank/EMBL data libraries under the following accession numbers: Plsp1 (At3g24590), OE33/PsbO1 (At5g66570), cpSecA1 (At4g01800), Cpn60 α1 (P08926/Psat7g144320), Cpn60 β1 (P08927/Psat1g001680), Cpn20 (At5g20720), RbcL (P00875), and RbcS (P00870 and Q43832). Other protein sequences from LC-MS/MS analyses in Table 1 and Figure 2 include Cpn60 α2 (Psat7g128880), Cpn60 β1 (Psat1g001680/Psat6g016820), Cpn60 β4 (Psat2g080360), RbcL (P04717), RbcS 3A (P07689/Psat3g205240), ClpC (P35100/Psat7g039080), Hsp70 (Q02028/Psat1g222760), and Hsp90 (Psat2g102720).

Supplemental Data

Supplemental Figure 1. mPlsp1 is protected from proteinase K by Cpn60/Cpn20.

Supplemental Figure 2. Coomassie-stained BN-PAGE from the import-chase assay.

Supplemental Figure 3. The 180-kD and 550-kD complexes during the import-chase assay.

Supplemental Figure 4. Lincomycin suppresses the appearance of the 550-kD complex in an import-chase assay.

Supplemental Figure 5. Colored homology model of the Plsp1 catalytic domain.

Supplemental Figure 6. The formation of the 550-kD and 180-kD complexes does not require any of the Plsp1 sequences analyzed.

Supplemental Figure 7. Δβ1-2 remains thermolysin susceptible after a 30-min import.

Supplemental Figure 8. cpSecA1 does not pull down Cpn60 from a SE.

Supplemental Figure 9. Stromal concentrations of cpSecA1 and Cpn60 are high.

Supplemental Figure 10. High concentrations of protein do not inhibit integration of Plsp1.

Supplemental Figure 11. RbcL displacement is less effective at room temperature.

Supplemental Figure 12. Three models could explain the hand-off of Plsp1 from Cpn60 to cpSec1.

Supplemental Table 1. Primers used for cloning.

Supplemental Table 2. Cpn60 gene identifiers in *Pisum sativum* and Arabidopsis.

Supplemental Methods. Expanded procedures for protein purification and LC-MS/MS analysis.

Supplemental Data Set 1. Full list of proteins identified in $mPlsp1_{\Delta TMD}$ in vitro pulldown assays.

Supplemental Data Set 2. Full list of proteins identified in excised 550-kD and 700-kD complexes.

Supplemental Data Set 3. Statistical analysis data.

ACKNOWLEDGMENTS

We thank Joshua K. Endow for his critical feedback and advice on many experiments. Abdussalam Azem kindly provided a gift of the Cpn60 α1 and β1 constructs. Brett Phinney and Michelle Salami at the University of California(UC), Davis Proteomics Core Facility provided training, technical expertise, and assistance with sample preparation and analysis for LC-MS/MS experiments. Prakitchai Chotewutmontri provided advice on the use of lincomycin, and Manajit Hayer-Hartl and F. Ulrich Hartl gave critical feedback on chaperonin experiments, particularly the Rubisco displacement assay. We also thank Philipp Zerbe and Rebecca Roston

for their critical reading of this article. This work was supported by the Office of Basic Energy Sciences of the U.S. Department of Energy (grant DE-SC0017035 to S.M.T. and grant DE-FG02-08ER15963 to K.I.), the UC Davis Department of Plant Sciences (Graduate Student Research Assistantship and Henry A. Jastro Graduate Research Award to L.K.), and the UC Davis Department of Plant Biology (Stocking Fellowship to L.K.). This is the last of three research papers that were published in the past year in *The Plant Cell* listing as coauthor our friend, mentor, and colleague Kentaro Inoue, who was tragically killed in an accident three years ago. These papers were each born of his inspiration and ideas, and the first author of each was one of the three graduate students in his lab at the time of his death. To mark the end of this chapter of Kentaro's active contributions to science, we would like to dedicate this paper to his memory.

AUTHOR CONTRIBUTIONS

L.K., K.I., and S.M.T. designed the experiments; L.K. performed all experiments and analyzed the data; and L.K. and S.M.T. wrote the article.

Received April 20, 2020; revised August 11, 2020; accepted October 21, 2020; published October 22, 2020.

REFERENCES

Adam, Z., Aviv-Sharon, E., Keren-Paz, A., Naveh, L., Rozenberg, M., Savidor, A., and Chen, J. (2019). The chloroplast envelope protease FTSH11: Interaction with CPN60 and identification of potential substrates. Front Plant Sci **10:** 428.

Aigner, H., Wilson, R.H., Bracher, A., Calisse, L., Bhat, J.Y., Hartl, F.U., and Hayer-Hartl, M. (2017). Plant RuBisCo assembly in *E. coli* with five chloroplast chaperones including BSD2. Science **358:** 1272–1278.

Asher, A., Ganesan, I., Klasek, L., and Theg, S.M. (2018). Isolation of physiologically active thylakoids and their use in energy-dependent protein transport assays. J. Vis. Exp. **2018:** 58393.

Bai, C., Guo, P., Zhao, Q., Lv, Z., Zhang, S., Gao, F., Gao, L., Wang, Y., Tian, Z., Wang, J., Yang, F., and Liu, C. (2015). Protomer roles in chloroplast chaperonin assembly and function. Mol. Plant **8:** 1478–1492.

Barkan, A. (1993). Nuclear mutants of maize with defects in chloroplast polysome assembly have altered chloroplast RNA metabolism. Plant Cell **5:** 389–402.

Barraclough, R., and Ellis, R.J. (1980). Protein synthesis in chloroplasts. IX. Assembly of newly-synthesized large subunits into ribulose bishopshate carboxylase in isolated intact pea chloroplasts. Biochim. Biophys. Acta **608:** 19–31.

Bie, A.S., Cömert, C., Körner, R., Corydon, T.J., Palmfeldt, J., Hipp, M.S., Hartl, F.U., and Bross, P. (2020). An inventory of interactors of the human HSP60/HSP10 chaperonin in the mitochondrial matrix space. Cell Stress Chaperones **25:** 407–416.

Bigman, L.S., and Horovitz, A. (2019). Reconciling the controversy regarding the functional importance of bullet- and football-shaped GroE complexes. J. Biol. Chem. **294:** 13527–13529.

Bochkareva, E., Seluanov, A., Bibi, E., and Girshovich, A. (1996). Chaperonin-promoted post-translational membrane insertion of a multispanning membrane protein lactose permease. J. Biol. Chem. **271:** 22256–22261.

Bonk, M., Hoffmann, B., Von Lintig, J., Schledz, M., Al-Babili, S., Hobeika, E., Kleinig, H., and Beyer, P. (1997). Chloroplast import of four carotenoid biosynthetic enzymes in vitro reveals differential fates prior to membrane binding and oligomeric assembly. Eur. J. Biochem. **247:** 942–950.

Brundage, L., Hendrick, J.P., Schiebel, E., Driessen, A.J.M., and Wickner, W. (1990). The purified *E. coli* integral membrane protein SecY/E is sufficient for reconstitution of SecA-dependent precursor protein translocation. Cell **62:** 649–657.

Castanié-Cornet, M.-P., Bruel, N., and Genevaux, P. (2014). Chaperone networking facilitates protein targeting to the bacterial cytoplasmic membrane. Biochim. Biophys. Acta **1843:** 1442–1456.

Chen, G.G., and Jagendorf, A.T. (1994). Chloroplast molecular chaperone-assisted refolding and reconstitution of an active multisubunit coupling factor CF1 core. Proc. Natl. Acad. Sci. USA **91:** 11497–11501.

Cho, H., and Shan, S.O. (2018). Substrate relay in an Hsp70-cochaperone cascade safeguards tail-anchored membrane protein targeting. EMBO J. **37:** e99264.

Chotewutmontri, P., and Barkan, A. (2018). Multilevel effects of light on ribosome dynamics in chloroplasts program genome-wide and psbA-specific changes in translation. PLoS Genet. **14:** e1007555.

Chou, M.-L., Chu, C.-C., Chen, L.-J., Akita, M., and Li, H.M. (2006). Stimulation of transit-peptide release and ATP hydrolysis by a cochaperone during protein import into chloroplasts. J. Cell Biol. **175:** 893–900.

Cox, J., and Mann, M. (2008). MaxQuant enables high peptide identification rates, individualized p.p.b.-range mass accuracies and proteome-wide protein quantification. Nat. Biotechnol. **26:** 1367–1372.

Cranford-Smith, T., and Huber, D. (2018). The way is the goal: How SecA transports proteins across the cytoplasmic membrane in bacteria. FEMS Microbiol. Lett. **365:** fny093.

Danese, P.N., Murphy, C.K., and Silhavy, T.J. (1995). Multicopy suppression of cold-sensitive sec mutations in *Escherichia coli*. J. Bacteriol. **177:** 4969–4973.

Deaton, J., Sun, J., Holzenburg, A., Struck, D.K., Berry, J., and Young, R. (2004). Functional bacteriorhodopsin is efficiently solubilized and delivered to membranes by the chaperonin GroEL. Proc. Natl. Acad. Sci. USA **101:** 2281–2286.

de Gier, J.-W.L., Mansournia, P., Valent, Q.A., Phillips, G.J., Luirink, J., and von Heijne, G. (1996). Assembly of a cytoplasmic membrane protein in *Escherichia coli* is dependent on the signal recognition particle. FEBS Lett. **399:** 307–309.

del Alamo, M., Hogan, D.J., Pechmann, S., Albanese, V., Brown, P.O., and Frydman, J. (2011). Defining the specificity of cotranslationally acting chaperones by systematic analysis of mRNAs associated with ribosome-nascent chain complexes. PLoS Biol. **9:** e1001100.

Dempsey, B.R., Wrona, M., Moulin, J.M., Gloor, G.B., Jalilehvand, F., Lajoie, G., Shaw, G.S., and Shilton, B.H. (2004). Solution NMR structure and X-ray absorption analysis of the C-terminal zinc-binding domain of the SecA ATPase. Biochemistry **43:** 9361–9371.

Dickson, R., Weiss, C., Howard, R.J., Alldrick, S.P., Ellis, R.J., Lorimer, G., Azem, A., and Viitanen, P.V. (2000). Reconstitution of higher plant chloroplast chaperonin 60 tetradecamers active in protein folding. J. Biol. Chem. **275:** 11829–11835.

Endow, J.K., and Inoue, K. (2013). Stable complex formation of thylakoidal processing peptidase and PGRL1. FEBS Lett. **587:** 2226–2231.

Endow, J.K., Singhal, R., Fernandez, D.E., and Inoue, K. (2015). Chaperone-assisted post-translational transport of plastidic type I signal peptidase 1. J. Biol. Chem. **290:** 28778–28791.

Feiz, L., Williams-Carrier, R., Belcher, S., Montano, M., Barkan, A., and Stern, D.B. (2014). A protein with an inactive pterin-4a-

carbinolamine dehydratase domain is required for Rubisco biogenesis in plants. Plant J. **80:** 862–869.

Feiz, L., Williams-Carrier, R., Wostrikoff, K., Belcher, S., Barkan, A., and Stern, D.B. (2012). Ribulose-1,5-bis-phosphate carboxylase/oxygenase accumulation factor1 is required for holoenzyme assembly in maize. Plant Cell **24:** 3435–3446.

Flores-Pérez, Ú., Bédard, J., Tanabe, N., Lymperopoulos, P., Clarke, A.K., and Jarvis, P. (2016). Functional analysis of the Hsp93/ClpC chaperone at the chloroplast envelope. Plant Physiol. **170:** 147–162.

Gadagkar, S.R., and Call, G.B. (2015). Computational tools for fitting the Hill equation to dose-response curves. J. Pharmacol. Toxicol. Methods **71:** 68–76.

Génier, S., Degrandmaison, J., Moreau, P., Labrecque, P., Hébert, T.E., and Parent, J.-L. (2016). Regulation of GPCR expression through an interaction with CCT7, a subunit of the CCT/TRiC complex. Mol. Biol. Cell **27:** 3800–3812.

Gruber, R., and Horovitz, A. (2016). Allosteric mechanisms in chaperonin machines. Chem. Rev. **116:** 6588–6606.

Hauser, T., Bhat, J.Y., Miličić, G., Wendler, P., Hartl, F.U., Bracher, A., and Hayer-Hartl, M. (2015). Structure and mechanism of the Rubisco-assembly chaperone Raf1. Nat. Struct. Mol. Biol. **22:** 720–728.

Haward, S.R., Napier, J.A., and Gray, J.C. (1997). Chloroplast SecA functions as a membrane-associated component of the Sec-like protein translocase of pea chloroplasts. Eur. J. Biochem. **248:** 724–730.

Hayer-Hartl, M., Bracher, A., and Hartl, F.U. (2016). The GroEL-GroES chaperonin machine: A nano-cage for protein folding. Trends Biochem. Sci. **41:** 62–76.

Heldt, H.W. (1980). Measurement of metabolite movement across the envelope and of the pH in the stroma and the thylakoid space in intact chloroplasts. In Methods Enzymol., Volume **69, pp.** 604–613.

Hemmingsen, S.M., and Ellis, R.J. (1986). Purification and properties of ribulosebisphosphate carboxylase large subunit binding protein. Plant Physiol. **80:** 269–276.

Howitz, K.T., and McCarty, R.E. (1982). pH dependence and kinetics of glycolate uptake by intact pea chloroplasts. Plant Physiol. **70:** 949–952.

Hsu, S.-C., Endow, J.K., Ruppel, N.J., Roston, R.L., Baldwin, A.J., and Inoue, K. (2011). Functional diversification of thylakoidal processing peptidases in *Arabidopsis thaliana*. PLoS One **6:** e27258.

Huang, P.-K., Chan, P.-T., Su, P.-H., Chen, L.-J., and Li, H.M. (2016). Chloroplast Hsp93 directly binds to transit peptides at an early stage of the preprotein import process. Plant Physiol. **170:** 857–866.

Inoue, H., Li, M., and Schnell, D.J. (2013). An essential role for chloroplast heat shock protein 90 (Hsp90C) in protein import into chloroplasts. Proc. Natl. Acad. Sci. USA **110:** 3173–3178.

Inoue, K., Furbee, K.J., Uratsu, S., Kato, M., Dandekar, A.M., and Ikoma, Y. (2006). Catalytic activities and chloroplast import of carotenogenic enzymes from citrus. Physiol. Plant. **127:** 561–570.

Inoue, K., and Keegstra, K. (2003). A polyglycine stretch is necessary for proper targeting of the protein translocation channel precursor to the outer envelope membrane of chloroplasts. Plant J. **34:** 661–669.

Jaru-Ampornpan, P., Shen, K., Lam, V.Q., Ali, M., Doniach, S., Jia, T.Z., and Shan, S.O. (2010). ATP-independent reversal of a membrane protein aggregate by a chloroplast SRP subunit. Nat. Struct. Mol. Biol. **17:** 696–702.

Jensen, R.G., and Bahr, J.T. (1977). Ribulose 1, 5-bisphosphate carboxylase-oxygenase. Annu. Rev. Plant Physiol. **28:** 379–400.

Jewett, A.I., and Shea, J.-E. (2010). Reconciling theories of chaperonin accelerated folding with experimental evidence. Cell. Mol. Life Sci. **67:** 255–276.

Jiang, T., Oh, E.S., Bonea, D., and Zhao, R. (2017). HSP90C interacts with PsbO1 and facilitates its thylakoid distribution from chloroplast stroma in *Arabidopsis*. PLoS One **12:** e0190168.

Ke, X., Zou, W., Ren, Y., Wang, Z., Li, J., Wu, X., and Zhao, J. (2017). Functional divergence of chloroplast Cpn60α subunits during *Arabidopsis* embryo development. PLoS Genet. **13:** e1007036.

Kerner, M.J., Naylor, D.J., Ishihama, Y., Maier, T., Chang, H.-C., Stines, A.P., Georgopoulos, C., Frishman, D., Hayer-Hartl, M., Mann, M., and Hartl, F.U. (2005). Proteome-wide analysis of chaperonin-dependent protein folding in *Escherichia coli*. Cell **122:** 209–220.

Kim, J., Eichacker, L.A., Rudiger, W., and Mullet, J.E. (1994). Chlorophyll regulates accumulation of the plastid-encoded chlorophyll proteins P700 and D1 by increasing apoprotein stability. Plant Physiol. **104:** 907–916.

Kim, S.-R., Yang, J.-I., and An, G. (2013). OsCpn60α1, encoding the plastid chaperonin 60α subunit, is essential for folding of rbcL. Mol. Cells **35:** 402–409.

Klasek, L., and Inoue, K. (2016). Chapter seven: Dual protein localization to the envelope and thylakoid membranes within the chloroplast. In International Review of Cell and Molecular Biology, W.J. Kwang, ed, Volume **Vol. 323 (Cambridge, MA: Academic Press), pp.** 231–263.

Kreplak, J., et al. (2019). A reference genome for pea provides insight into legume genome evolution. Nat. Genet. **51:** 1411–1422.

Kusukawa, N., Yura, T., Ueguchi, C., Akiyama, Y., and Ito, K. (1989). Effects of mutations in heat-shock genes groES and groEL on protein export in *Escherichia coli*. EMBO J. **8:** 3517–3521.

Lecker, S., Lill, R., Ziegelhoffer, T., Georgopoulos, C., Bassford, P.J., Jr., Kumamoto, C.A., and Wickner, W. (1989). Three pure chaperone proteins of *Escherichia coli*—SecB, trigger factor and GroEL—form soluble complexes with precursor proteins in vitro. EMBO J. **8:** 2703–2709.

Li, L., Nelson, C.J., Trösch, J., Castleden, I., Huang, S., and Millar, A.H. (2017). Protein degradation rate in *Arabidopsis thaliana* leaf growth and development. Plant Cell **29:** 207–228.

Liu, C., Young, A.L., Starling-Windhof, A., Bracher, A., Saschenbrecker, S., Rao, B.V., Rao, K.V., Berninghausen, O., Mielke, T., Hartl, F.U., Beckmann, R., and Hayer-Hartl, M. (2010). Coupled chaperone action in folding and assembly of hexadecameric Rubisco. Nature **463:** 197–202.

Lorimer, G.H. (1996). A quantitative assessment of the role of the chaperonin proteins in protein folding in vivo. FASEB J. **10:** 5–9.

Lubben, T.H., Donaldson, G.K., Viitanen, P.V., and Gatenby, A.A. (1989). Several proteins imported into chloroplasts form stable complexes with the GroEL-related chloroplast molecular chaperone. Plant Cell **1:** 1223–1230.

Ma, X. (2000). Protein targeting and translocation on cpSEC and Delta pH pathways in chloroplast thylakoids. PhD dissertation (Gainesville, FL: University of Florida).

Madueno, F., Napier, J.A., and Gray, J.C. (1993). Newly imported Rieske iron-sulfur protein associates with both Cpn60 and Hsp70 in the chloroplast stroma. Plant Cell **5:** 1865–1876.

Mao, J., Chi, W., Ouyang, M., He, B., Chen, F., and Zhang, L. (2015). PAB is an assembly chaperone that functions downstream of chaperonin 60 in the assembly of chloroplast ATP synthase coupling factor 1. Proc. Natl. Acad. Sci. USA **112:** 4152–4157.

McKinnon, L.J., Fukushima, J., Endow, J.K., Inoue, K., and Theg, S.M. (2020). Membrane chaperoning of a thylakoid protease whose

structural stability is modified by the protonmotive force. Plant Cell **32:** 1589–1609.

Molik, S., Karnauchov, I., Weidlich, C., Herrmann, R.G., and Klösgen, R.B. (2001). The Rieske Fe/S protein of the cytochrome b6/f complex in chloroplasts: Missing link in the evolution of protein transport pathways in chloroplasts? J. Biol. Chem. **276:** 42761–42766.

Musgrove, J.E., Johnson, R.A., and Ellis, R.J. (1987). Dissociation of the ribulosebisphosphate-carboxylase large-subunit binding protein into dissimilar subunits. Eur. J. Biochem. **163:** 529–534.

Nakai, M., Goto, A., Nohara, T., Sugita, D., and Endo, T. (1994). Identification of the SecA protein homolog in pea chloroplasts and its possible involvement in thylakoidal protein transport. J. Biol. Chem. **269:** 31338–31341.

Nishimura, K., and van Wijk, K.J. (2015). Organization, function and substrates of the essential Clp protease system in plastids. Biochim. Biophys. Acta **1847:** 915–930.

Nishio, K., Hirohashi, T., and Nakai, M. (1999). Chloroplast chaperonins: evidence for heterogeneous assembly of α and β Cpn60 polypeptides into a chaperonin oligomer. Biochem. Biophys. Res. Commun. **266:** 584–587.

Olinares, P.D.B., Ponnala, L., and van Wijk, K.J. (2010). Megadalton complexes in the chloroplast stroma of *Arabidopsis thaliana* characterized by size exclusion chromatography, mass spectrometry, and hierarchical clustering. Mol. Cell. Proteomics **9:** 1594–1615.

Payan, L.A., and Cline, K. (1991). A stromal protein factor maintains the solubility and insertion competence of an imported thylakoid membrane protein. J. Cell Biol. **112:** 603–613.

Paetzel, M. (2014). Structure and mechanism of *Escherichia coli* type I signal peptidase. Biochim. Biophys. Acta **1843:** 1497–1508.

Peltier, J.-B., Cai, Y., Sun, Q., Zabrouskov, V., Giacomelli, L., Rudella, A., Ytterberg, A.J., Rutschow, H., and van Wijk, K.J. (2006). The oligomeric stromal proteome of *Arabidopsis thaliana* chloroplasts. Mol. Cell. Proteomics **5:** 114–133.

Peng, L., Fukao, Y., Myouga, F., Motohashi, R., Shinozaki, K., and Shikanai, T. (2011). A chaperonin subunit with unique structures is essential for folding of a specific substrate. PLoS Biol. **9:** e1001040.

Phillips, G.J., and Silhavy, T.J. (1990). Heat-shock proteins DnaK and GroEL facilitate export of LacZ hybrid proteins in E. coli. Nature **344:** 882–884.

Pradel, N., Delmas, J., Wu, L.F., Santini, C.L., and Bonnet, R. (2009). Sec- and Tat-dependent translocation of β-lactamases across the *Escherichia coli* inner membrane. Antimicrob. Agents Chemother. **53:** 242–248.

Rast, A., Heinz, S., and Nickelsen, J. (2015). Biogenesis of thylakoid membranes. Biochim Biophys Acta Bioenerg **1847:** 821–830.

Rast, A., Schaffer, M., Albert, S., Wan, W., Pfeffer, S., Beck, F., Plitzko, J.M., Nickelsen, J., and Engel, B.D. (2019). Biogenic regions of cyanobacterial thylakoids form contact sites with the plasma membrane. Nat. Plants **5:** 436–446.

Robinson, S.P. (1984). Lack of ATP requirement for light stimulation of glycerate transport into intact isolated chloroplasts. Plant Physiol. **75:** 425–430.

Rosano, G.L., Bruch, E.M., and Ceccarelli, E.A. (2011). Insights into the Clp/HSP100 chaperone system from chloroplasts of *Arabidopsis thaliana*. J. Biol. Chem. **286:** 29671–29680.

Rutschow, H., Ytterberg, A.J., Friso, G., Nilsson, R., and van Wijk, K.J. (2008). Quantitative proteomics of a chloroplast SRP54 sorting mutant and its genetic interactions with CLPC1 in Arabidopsis. Plant Physiol. **148:** 156–175.

Sala, A., Bordes, P., and Genevaux, P. (2014). Multitasking SecB chaperones in bacteria. Front. Microbiol. **5:** 666.

Schibich, D., Gloge, F., Pöhner, I., Björkholm, P., Wade, R.C., von Heijne, G., Bukau, B., and Kramer, G. (2016). Global profiling of SRP interaction with nascent polypeptides. Nature **536:** 219–223.

Schmid, M., Davison, T.S., Henz, S.R., Pape, U.J., Demar, M., Vingron, M., Schölkopf, B., Weigel, D., and Lohmann, J.U. (2005). A gene expression map of *Arabidopsis thaliana* development. Nat. Genet. **37:** 501–506.

Schneider, C.A., Rasband, W.S., and Eliceiri, K.W. (2012). NIH Image to ImageJ: 25 years of image analysis. Nat. Methods **9:** 671–675.

Shan, S.-o. (2019). Guiding tail-anchored membrane proteins to the endoplasmic reticulum in a chaperone cascade. J. Biol. Chem. **294:** 16577–16586.

Shi, L.X., and Theg, S.M. (2010). A stromal heat shock protein 70 system functions in protein import into chloroplasts in the moss *Physcomitrella patens*. Plant Cell **22:** 205–220.

Shipman, R.L., and Inoue, K. (2009). Suborganellar localization of plastidic type I signal peptidase 1 depends on chloroplast development. FEBS Lett. **583:** 938–942.

Su, P.-H., and Li, H.M. (2010). Stromal Hsp70 is important for protein translocation into pea and Arabidopsis chloroplasts. Plant Cell **22:** 1516–1531.

Sun, Q., Zybailov, B., Majeran, W., Friso, G., Olinares, P.D.B., and van Wijk, K.J. (2009). PPDB, the plant proteomics database at Cornell. Nucleic Acids Res. **37:** D969–D974.

Suzuki, K., Nakanishi, H., Bower, J., Yoder, D.W., Osteryoung, K.W., and Miyagishima, S.Y. (2009). Plastid chaperonin proteins Cpn60 α and Cpn60 β are required for plastid division in *Arabidopsis thaliana*. BMC Plant Biol. **9:** 38.

Takabayashi, A., Takabayashi, S., Takahashi, K., Watanabe, M., Uchida, H., Murakami, A., Fujita, T., Ikeuchi, M., and Tanaka, A. (2017). PCoM-DB update: A protein co-migration database for photosynthetic organisms. Plant Cell Physiol. **58:** e10.

Tian, G.-W., et al. (2004). High-throughput fluorescent tagging of full-length Arabidopsis gene products in planta. Plant Physiol. **135:** 25–38.

Tsugeki, R., and Nishimura, M. (1993). Interaction of homologues of Hsp70 and Cpn60 with ferredoxin-NADP+ reductase upon its import into chloroplasts. FEBS Lett. **320:** 198–202.

Valent, Q.A., Scotti, P.A., High, S., de Gier, J.-W.L., von Heijne, G., Lentzen, G., Wintermeyer, W., Oudega, B., and Luirink, J. (1998). The *Escherichia coli* SRP and SecB targeting pathways converge at the translocon. EMBO J. **17:** 2504–2512.

Van Dyk, T.K., Gatenby, A.A., and LaRossa, R.A. (1989). Demonstration by genetic suppression of interaction of GroE products with many proteins. Nature **342:** 451–453.

Viitanen, P.V., Schmidt, M., Buchner, J., Suzuki, T., Vierling, E., Dickson, R., Lorimer, G.H., Gatenby, A., and Soll, J. (1995). Functional characterization of the higher plant chloroplast chaperonins. J. Biol. Chem. **270:** 18158–18164.

Vitlin, A., Weiss, C., Demishtein-Zohary, K., Rasouly, A., Levin, D., Pisanty-Farchi, O., Breiman, A., and Azem, A. (2011). Chloroplast β chaperonins from *A. thaliana* function with endogenous cpn10 homologs in vitro. Plant Mol. Biol. **77:** 105–115.

Vitlin Gruber, A., and Feiz, L. (2018). Rubisco assembly in the chloroplast. Front. Mol. Biosci. **5:** 24.

Vitlin Gruber, A., Zizelski, G., Azem, A., and Weiss, C. (2014). The Cpn10(1) co-chaperonin of *A. thaliana* functions only as a hetero-oligomer with Cpn20. PLoS One **9:** e113835.

Weiss, C., Jebara, F., Nisemblat, S., and Azem, A. (2016). Dynamic complexes in the chaperonin-mediated protein folding cycle. Front. Mol. Biosci. **3:** 80.

Weissman, J.S., Hohl, C.M., Kovalenko, O., Kashi, Y., Chen, S., Braig, K., Saibil, H.R., Fenton, W.A., and Horwich, A.L. (1995).

Mechanism of GroEL action: Productive release of polypeptide from a sequestered position under GroES. Cell **83:** 577–587.

Yam, A.Y., Xia, Y., Lin, H.-T.J., Burlingame, A., Gerstein, M., and Frydman, J. (2008). Defining the TRiC/CCT interactome links chaperonin function to stabilization of newly made proteins with complex topologies. Nat. Struct. Mol. Biol. **15:** 1255–1262.

Zabaleta, E., Oropeza, A., Assad, N., Mandel, A., Salerno, G., and Herrera-Estrella, L. (1994). Antisense expression of chaperonin 60β in transgenic tobacco plants leads to abnormal phenotypes and altered distribution of photoassimilates. Plant J. **6:** 425–432.

Zhao, Q., and Liu, C. (2018). Chloroplast chaperonin: An intricate protein folding machine for photosynthesis. Front. Mol. Biosci. **4:** 98.

Zhao, Q., Zhang, X., Sommer, F., Ta, N., Wang, N., Schroda, M., Cong, Y., and Liu, C. (2019). Hetero-oligomeric CPN60 resembles highly symmetric group-I chaperonin structure revealed by Cryo-EM. Plant J. **98:** 798–812.

Zoschke, R., and Barkan, A. (2015). Genome-wide analysis of thylakoid-bound ribosomes in maize reveals principles of co-translational targeting to the thylakoid membrane. Proc. Natl. Acad. Sci. USA **112:** E1678–E1687.